PAPER

Emergent complex quantum networks in continuous-variables non-Gaussian states

To cite this article: Mattia Walschaers et al 2023 Quantum Sci. Technol. 8 035009

View the article online for updates and enhancements.

You may also like

- Atomic step-and-terrace surface of polyimide sheet for advanced polymer substrate engineering
 G Tan, K Shimada, Y Nozawa et al.
- <u>Soft-molecular imprinted electrospun</u> <u>scaffolds to mimic specific biological</u> <u>tissues</u> Giuseppe Criscenti, Carmelo De Maria, Alessia Longoni et al.
- Imprinting Sensor Based on Honeycomb Graphene Oxide for the Determination of Echinacoside in Complex Samples Jing Ma, YanPing Wang, Xiumei Zhu et al.

Quantum Science and Technology



RECEIVED

22 November 2022

REVISED

27 March 2023

ACCEPTED FOR PUBLICATION 18 April 2023

PUBLISHED
4 May 2023

PAPER

Emergent complex quantum networks in continuous-variables non-Gaussian states

Mattia Walschaers^{1,*}, Bhuvanesh Sundar², Nicolas Treps¹, Lincoln D Carr^{3,4}

- ¹ Laboratoire Kastler Brossel, Sorbonne Université, CNRS, ENS-Université PSL, Collège de France, 4 place Jussieu, F-75252 Paris, France
- Institute for Quantum Optics and Quantum Information of the Austrian Academy of Sciences, Innsbruck A 6020, Austria
- Quantum Engineering Program, Colorado School of Mines, Golden, Colorado CO 80401, United States of America
- Department of Physics, Colorado School of Mines, Golden, CO 80401, United States of America
- * Author to whom any correspondence should be addressed.

E-mail: mattia.walschaers@lkb.upmc.fr and valentina.parigi@lkb.upmc.fr

Keywords: complex networks, quantum optics, continuous variables, cluster states, non-Gaussian quantum states

Abstract

We use complex network theory to study a class of photonic continuous variable quantum states that present both multipartite entanglement and non-Gaussian statistics. We consider the intermediate scale of several dozens of modes at which such systems are already hard to characterize. In particular, the states are built from an initial *imprinted* cluster state created via Gaussian entangling operations according to a complex network structure. We then engender non-Gaussian statistics via multiple photon subtraction operations acting on a single node. We replicate in the quantum regime some of the models that mimic real-world complex networks in order to test their structural properties under local operations. We go beyond the already known single-mode effects, by studying the *emergent* network of photon-number correlations via complex networks measures. We analytically prove that the imprinted network structure defines a vicinity of nodes, at a distance of four steps from the photon-subtracted node, in which the emergent network changes due to photon subtraction. We show numerically that the emergent structure is greatly influenced by the structure of the imprinted network. Indeed, while the mean and the variance of the degree and clustering distribution of the emergent network always increase, the higher moments of the distributions are governed by the specific structure of the imprinted network. Finally, we show that the behaviour of nearest neighbours of the subtraction node depends on how they are connected to each other in the imprinted structure.

1. Introduction

Large multiparty quantum systems are extremely hard to describe, although the complex behavior of their quantum states is what makes them appealing resources for quantum information processing. Intensive efforts have been dedicated to the direct representation of quantum states via numerical and analytical approaches with the aim of classifying and detecting truly non-classical and useful quantum features, like entanglement [1, 2].

In this work we focus on the complex behaviour of quantum states in continuous variable (CV) quantum systems and we tackle it via complex network theory. Our work is motivated by all-optical platforms, based on continuous quantum observables, that can already produce large entangled networks [3–5]. These networks are made of traveling light fields with quantum correlations between amplitude and phase values of different modes of the field, e.g. light at different colors. They have Gaussian measurement statistics for amplitude and phase continuous variables, so that they can be easily simulated via classical computer. They are essential resources for measurement-based quantum computing but, in order to perform quantum protocols, they must acquire non-Gaussian statistics of the continuous variables. Non-Gaussian statistics can be induced via mode-selective addition and subtraction of photons [6, 7], that are then called non-Gaussian

operations. When the number of entangled systems—in our case optical modes—and the number of non-Gaussian operations grow, these systems quickly become hard to benchmark [8–13].

In the most general scenario, even measurement outcomes of such systems become computationally hard to simulate [14], so that the associated sampling problem is one of the many variations of bosons sampling [15, 16]. This connection is made particularly clear when one considers a more general state preparation framework based on photon-number-resolving detectors of which photon multi-photon-subtraction and Gaussian boson sampling are limiting cases [17]. Such sampling setups have recently led to several demonstrations of a quantum computational advantage [18–20]. It was shown that for bosonic sampling setups the computational complexity is governed by the number photons that are detected or injected in the setup [21]. This emphasises the potential importance of multi-photon-subtracted states and of finding way to characterise them. Photon-number correlations have shown to be efficient tools to extract properties of such intricate systems [18–20, 22–25]. Average values of photon-number correlations can be analytically tractable, but they can only unveil global properties of the system. Yet, to acquire a more detailed image of the state, we can use network theory to analyse distributions of photon-number correlations.

In this work, the use of network theory will be two-fold. First, the optical CV entangled networks can in fact be easily reconfigured in arbitrary shape [26]. We can thus consider entangled networks which are generated through models studied in network theory to reproduce the features of real-world networks. They provide an excellent playground to explore whether mimicking real-world complex network structures [27, 28] provides an advantage for quantum information technologies, including quantum simulation and communication [26, 29] in a future quantum internet. Second, we will use network theory as a powerful tool for benchmarking entangled networks when affected by local non-Gaussian operations by building weighted networks of photon-number correlations. We can then study how different shapes of the initial entangled network can support, enhance, spread or destroy the non-Gaussian features provided by local subtraction of multiple photons. By subtracting all the photons in the same mode, we keep the problem computationally tractable for a numerical study. To explore the scenario where many photons are subtracted in many modes, one would require a quantum device because those systems cannot be efficiently simulated on classical hardware.

1.1. Conceptual scheme

The conceptual scheme of our analysis is shown in figure 1. Large CV entangled networks have been deterministically implemented via non-linear $\chi^{(2)}$ optical processes. This operation entangles different modes (be they spatial, spectral or temporal) of the fields via an appropriately engineered parametric interaction [3–5, 26, 30, 31]. These processes are sketched in the left corner of the upper row of figure 1, where the different modes are represented by different colors. The circuit representation of the generated states is sketched in the second row of the figure: the non-linear optical process is equivalent to different travelling optical modes occupied by squeezed vacuum states that are entangled via C_Z gates. This generates the cluster state [32, 33]. In the third row we show the graphical representation of the state: the different optical modes are represented by different nodes of the network which are linked by C_Z gate entangling operations, counted by the entry 1 in the adjacency matrix \mathcal{A} of the network. This structure is an *imprinted* network, as it builds the initial quantum states. In the right side of the first column of figure 1 we picture the action of multiple-photon subtraction, i.e. the repeated application of the photon annihilation operator \hat{a} on one specific mode of the field. The probabilistic implementation of this operation consists of a mode-selective beam-splitter that sends a small fraction of light to a photon counter: when *n* photons are detected an n-photon-subtracted state is heralded. The process can be implemented via non-linear interaction with supplementary gate fields [6]. In the fourth row of the first column we show the network of photon-number correlations between the different field modes that emerge from the imprinted network. This is the *emergent* network. Its adjacency matrix A contains continuous values between 0 and 1, indicating the strength of photon-number correlations between couple of nodes. In this work we are interested in following the changes of this emergent network of photon number correlations after photon-subtractions on one node as a benchmark of the desired non-Gaussian properties of CV quantum states.

1.2. Summary of the results

The entangling C_Z -gates in the imprinted network generate short range correlations between nodes. Also, the non-Gaussian operations we consider here—photon-subtractions—are applied locally on a single node. Under such conditions the effect of photon subtraction on a regular graph is limited [34]. On the contrary, here we probe imprinted networks constructed from complex network models, where typical distances between nodes are short. Our results are as follows:

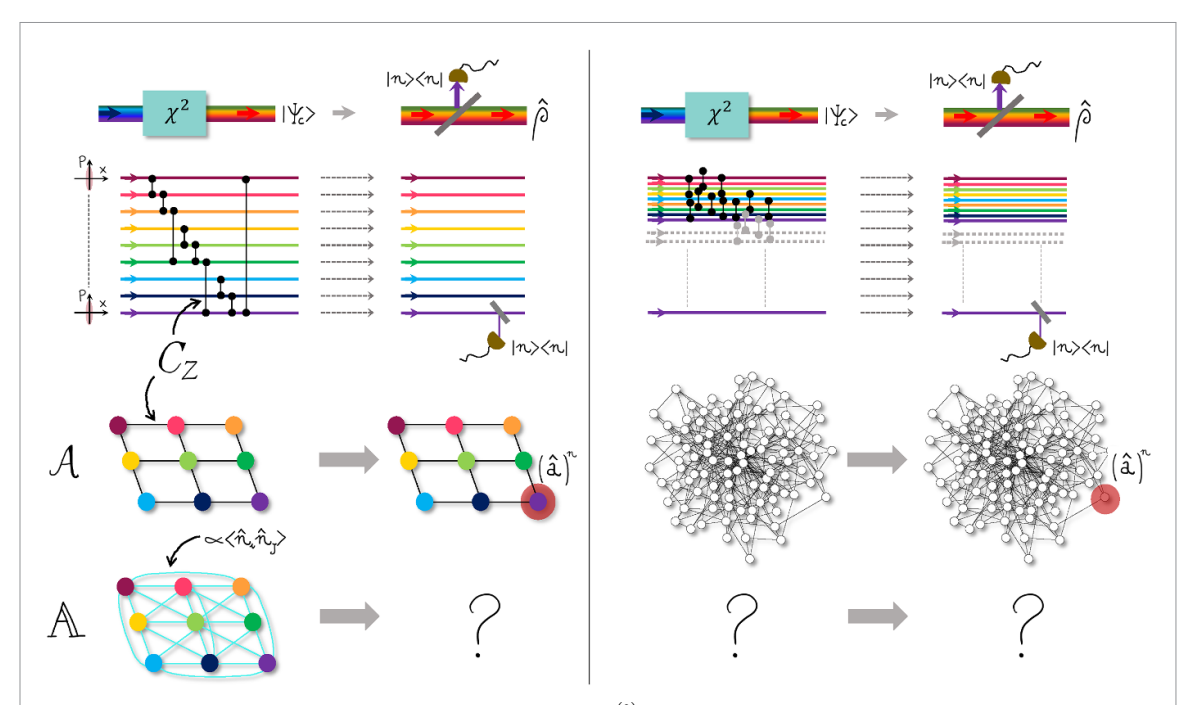


Figure 1. Left column, first row: sketch of nonlinear multi-mode $\chi^{(2)}$ optical processes that demonstrate the deterministic implementation of large CV networks and mode-dependent multi-photon subtraction. Second row: circuit representation of the two processes. Third row: graphical representation of the so-called cluster states (imprinted networks) where the nodes are the different modes of the field and edges correspond to C_Z gates between modes. Last and fourth row: emergent networks where edges are photon-number correlations between modes. Right column: same as left but considering imprinted cluster with shapes typical of complex network models.

- For imprinted complex networks we see highly connected emergent networks of photon-number correlations
- The imprinted network structure defines a vicinity of nodes around the photon-subtracted node in which the emergent network changes due to photon subtraction.
- Some networks are more efficient than others in spreading the non-Gaussian features. This depends on the amount of randomness and on the inhomogeneity of number of links in their structure.
- The properties of the emergent networks after photon subtraction are mainly dictated by the local network structure in the vicinity of the photon subtraction node.

1.3. Structure of the paper

The Article is outlined as follows. Section 2 introduces the basic concepts of complex networks and CV cluster states used in this work to make the Article accessible to readers with different backgrounds—readers with one or both areas of expertise may choose to skip this section or particular subsections. We describe the imprinted network structure and review non-Gaussian operations and their importance for getting non-Gaussian CV cluster states. We introduce the emergent correlation networks and complex network measures. Then in section 3 we look at emergent correlation networks for Gaussian cluster states when different complex network models are used for the imprinted network. This section forms a baseline for the ensuing non-Gaussian analysis. In section 4 we describe the evolution of the emergent correlation networks when repeated photon subtractions are applied. We show that photon subtraction in a single node only affects a certain vicinity of the subtraction node. We then analyse the global impact of the non-Gaussian operation on the emergent network. In section 5 we analyse the local effects of photon subtraction. We show that the sub-networks formed by nodes at different distances from the subtracting point have a different influence on the statistics of the non-Gaussian graphs. We then reveal the driving mechanism for the sub-networks composed by all the node at distance one from the subtracting point, i.e. all the nodes that have a direct link with the subtracting node in the imprinted network. Finally, in section 6 we comment on general features of non-Gaussian correlations in photon-subtracted networks and specific features dependent on the imprinted network model.

2. Quantum complex network theory and continuous variable quantum systems

2.1. Complex networks and quantum physics

In the last decades, network theory has made significant progress in describing collective features and functionality of complex systems [35, 36]. Network-based descriptions are pivotal in social and biological science as well as in technological infrastructures like power grids and information networks such as the internet. The study of complex network structures has spread in physics [37, 38] helping in the description of complex physical systems. Subfields in physics utilizing complex networks include statistical physics, condensed matter and quantum physics with, e.g. the study of the Ising model and Bose Einstein condensation [39-45]. More recently the study of complex networks has become relevant for quantum systems and procedures employed in quantum information technologies [27, 28, 46-50] indicating that a dedicated theory of quantum complex networks needs to be built, especially for networks with no classical equivalent, like those based on quantum correlations or quantum mutual information. In particular, emergent complex networks based on quantum mutual information have determined critical points for quantum phase transitions [44, 51, 52]. Likewise, complex network theory has been successful in determining self-similarity in entanglement structure of spin-chains [53] as well as new kinds of structured entanglement emerging from quantum cellular automata [54] on qubit/gate/ciruit-based quantum computers. Networks are naturally evoked in the quantum regime in relation to the quantum internet [55], where it is not clear yet if the best arrangement of its components will take a complex shape like the classical internet. Networks are however pivotal in all quantum technologies. Indeed, quantum information algorithms and quantum transport can be mapped to quantum walks on regular and complex networks [56–59]. Complex networks have also a crucial role in near-term quantum information processing because they describe networked noisy intermediate-scale quantum computers [60, 61]. Thus complex network theory provides a versatile toolbox, as it can be applied to different quantum features, and is very efficient in revealing emerging collective structural mechanisms.

Here we apply, for the first time, complex network analysis to CV multipartite quantum states. We focus on the ones that can be generated in the more advanced optical platforms, but the method can be applied to general CV states.

Networks are a collection of nodes and links. This is a very versatile conceptual structure that can be applied to any kind of relation between a collection of physical systems: receivers and senders in an information network linked by physical channels; atomic spins interacting via magnetic forces; or physical observables linked by correlation relations. The adjacency matrix is the central mathematical object of complex network theory: a non-zero term in the matrix indicates a link between two nodes, where the indices of the matrix determine the nodes. The work done in this Article is based on constructing the adjacency matrices for relevant networks, and subsequently extracting relevant properties from them.

In quantum information, graphs define the structure of the so-called *graph* or *cluster states*⁵. They correspond to multipartite quantum states with a specific entanglement structure introduced in the context of measurement-based quantum computing [32, 33, 62, 63]. For such cluster states, a non-zero term in the adjacency matrix indicates that an entangling gate has been applied between two qubits or between two quantum fields in two different optical modes (where the information is encoded in discrete or continuous variables, respectively). We first provide a brief introduction to CV quantum optics in section 2.2 and we review the CV cluster states that are induced by the imprinted networks in section 2.3. Then in section 2.4 we introduce the photon subtraction operation that creates non-Gaussian features in these quantum states. We define the emergent network of photon-number correlations in section 2.5. Finally, in section 2.6 we review network measures in the context of complex network models.

2.2. Continuous variable quantum optics

A *m*-mode light field [64] can be described as an ensemble of *m* quantum harmonic oscillators with creation and annihilation operators which obey the commutation relation $[\hat{a}_j, \hat{a}_k^{\dagger}] = \delta_{j,k}$. In the CV framework, we focus on 'position' and 'momentum' variables of these harmonic oscillators, $\hat{x}_k = \hat{a}_k^{\dagger} + \hat{a}_k$ and $\hat{p}_k = i(\hat{a}_k^{\dagger} - \hat{a}_k)$, also called *quadratures*. Generic quantum states of such quantum harmonic oscillators are hard to characterize, but the subclass of Gaussian states is very well understood. These states are completely described by the quadrature expectation values (the mean field) and covariance matrix *V*. To define the latter, let us introduce the 2*m*-dimensional vector $\vec{\xi} = (\hat{x}_1, \dots, \hat{x}_m, \hat{p}_1, \dots \hat{p}_m)^{\top}$, and introduce

⁵ Cluster is sometimes reserved for graphs allowing for universal quantum computing. In this work, however, we use the terms *cluster state* and *graph state* as synonyms.

$$V = \operatorname{Re} \langle \hat{\xi} \, \hat{\xi}^{\top} \rangle - \langle \hat{\xi} \rangle \langle \hat{\xi}^{\top} \rangle, \tag{1}$$

where $\langle . \rangle$ denotes the expectation value of the observables in the state ρ . If this state is Gaussian, all its higher order correlations can be expressed in terms of V [65] (note that this property is explicitly used in appendix A).

In this work, we will associate specific optical modes with the nodes of a network, as shown in figure 1. Such networks are naturally realized in the cluster state formalism of CV measurement-based quantum computing. It was experimentally demonstrated that such cluster states can be generated in arbitrary shapes [26].

2.3. Clusters: imprinted quantum networks

In quantum optics ideal cluster states require infinite energy to produce, it is therefor common to consider approximate cluster states, based on applying C_Z gates on a set of squeezed vacuum modes. The finitely squeezed states can be written as $\hat{S}(s)|0\rangle^{\bigotimes N}$, where $\hat{S}(s)$ is the squeezing operator, and $|0\rangle$ the vacuum state. The parameter s>1 denotes the squeezing, which for simplicity is chosen to be the same in all N copies. The unitary C_Z gates that entangle these squeezed vacuum modes are given by $C_Z = \exp(\imath \hat{x}_i \otimes \hat{x}_j)$.

This results in a Gaussian state with covariance matrix (1) given by $V_s = \operatorname{diag}[s, \dots, s, 1/s, \dots, 1/s]$. The first N elements in the diagonal are the variances of the x quadrature of the N modes (nodes) $\langle \hat{x}_i^2 \rangle = s \langle \hat{x}^2 \rangle_v = s$ where $\langle x^2 \rangle_v$ is the variance of the quadrature for the vacuum state which is taken equal to 1. The last N elements are the variances of the p quadrature $\langle \hat{p}_i^2 \rangle = 1/s$ of the N modes. The approximate cluster state that results by acting on $\hat{S}(s)|0\rangle^{\bigotimes N}$ with a network of C_Z gates is then described by [66]:

$$V = \begin{pmatrix} V_{xx} & V_{xp} \\ V_{px} & V_{pp} \end{pmatrix} = \begin{pmatrix} \mathbb{1} & 0 \\ \mathcal{A} & \mathbb{1} \end{pmatrix} V_s \begin{pmatrix} \mathbb{1} & \mathcal{A} \\ 0 & \mathbb{1} \end{pmatrix} = \begin{pmatrix} s\mathbb{1} & s\mathcal{A} \\ s\mathcal{A} & s\mathcal{A}^2 + \mathbb{1}/s \end{pmatrix}. \tag{2}$$

Here, V is a $2N \times 2N$ matrix divided into four $N \times N$ blocks. V_{xx} and V_{pp} describe the correlations among the x- and p-quadratures, respectively, whereas V_{xp} and V_{px} contain all correlations between x- and p-quadratures. The presence of \mathcal{A}^2 in V_{pp} highlights that correlations extend not only between nearest neighbor nodes, but also between next-nearest neighbors of the imprinted network. The elements $[\mathcal{A}^2]_{ij}$ are in fact known to correspond to the number of walks of exactly two steps from j to i of the network \mathcal{A} [33, 34].

The C_Z gates, which create the entanglement, can be implemented according to any network shape, i.e. any adjacency matrix \mathcal{A} . When used in measurement-based quantum computing, cluster states are built to ensure persistence of entanglement [67]. This means that a measurement on one node only locally affects the state and the surviving entanglement links can be further exploited for the next steps in measurement-based computing. To this end, some regular 2D graph structures, e.g. hexagonal or triangular lattices, have been proven to allow for universal computing. That is, arbitrary unitary operations can be performed via local operations and classical communication on the cluster. In contrast, others have been discarded, e.g. the tree graph [68]. Here we go beyond such regular structures, motivated by the fact that CV quantum networks in optical setups can be easily reconfigured to arbitrary shapes [26]. We want to indeed replicate in the quantum regime some of the models that mimic real-world complex networks [27, 28] in order to test their structural properties under local operations.

In the remainder of the Article we refer to the network that describes the pattern A of C_Z gates that are applied to create the Gaussian cluster state as the *imprinted network*.

2.4. Non-Gaussian operations in continuous variable platforms

Cluster states are characterized by Gaussian statistics of quadrature measurements, which allows for a compact statistical description even when they have a large size. However, for quantum computing protocols, cluster states must also acquire non-Gaussian quadrature statistics via non-Gaussian operations. Unlike the Gaussian case, the quantum features of such non-Gaussian networks are not trivial to classify [34, 69, 70]. Examples of non-Gaussian operations are the conditional implementation of single-photon subtraction and addition, i.e. the action of annihilation and creation operators \hat{a} and \hat{a}^{\dagger} [6, 7, 71–75]. Such operations have long been investigated as primitive for two important operations for quantum protocols: entanglement distillation and the generation of Wigner negativity. Single-photon subtraction and addition can also be combined to engender high-order non-Gaussian operations [9, 11, 76, 77].

In this Article, we focus on multi-photon-subtraction operations that can ideally be represented, in a multimode case, by the following operation on a state ρ :

$$\rho \mapsto \frac{\hat{a}_{S_n} \dots \hat{a}_{S_1} \rho \hat{a}_{S_1}^{\dagger} \dots \hat{a}_{S_n}^{\dagger}}{\operatorname{tr}[\hat{a}_{S_1}^{\dagger} \dots \hat{a}_{S_n}^{\dagger} \hat{a}_{S_n} \dots \hat{a}_{S_1} \rho]},\tag{3}$$

where S_i denotes a particular mode. In general, equation (3) describes repeated subtractions from different nodes, or even from superpositions of different nodes, that have recently been experimentally implemented [6, 71]. When these operations are applied on multimode quantum states characterization of the resulting states is not a trivial task. Recent results have depicted the rules of thumb for entanglement and Wigner negativity [8, 34, 69, 70], indicating that a deeper structural analysis would be beneficial for a more comprehensive picture.

Here, we specifically consider repeated photon subtractions from one single node of the cluster state in equation (2). There are two main reasons for this choice. First, we focus on the simplest scheme providing significant statistics. In fact, when multiple subtractions from an arbitrary superposition of nodes are considered, the analysis becomes computationally hard [14]. Second, we aim at probing the extent of the effect of photon subtraction in the most local way possible. In previous work, we have shown that photon subtraction on a given node induces non-Gaussian features in its nearest and next-to-nearest neighbor nodes [34]. This Article goes beyond single-point features such as local averages. Instead, we focus on the changes induced in the *correlations* between those nodes, including *beyond* next-nearest neighbors. We then study how different imprinted network shapes \mathcal{A} spread or destroy the non-Gaussian features created by photon subtraction. This is a problem that is very typical for classical information networks, studied here in the new context of quantum correlations.

2.5. Emergent complex networks of photon number correlations

Covariance matrices are sufficient to explain the behaviour of Gaussian states. In the case of non-Gaussian states expectation values of higher order operators are needed. In this Article, we focus on photon-number correlations, that are simple non-Gaussian observables with a clear physical interpretation. Photon number correlations can be written in terms of fourth moments of quadratures, which are sensitive to the non-Gaussianity—i.e. departure from Gaussian shape—of the quadrature distribution [8].

To consider structural effects, we introduce a second network for each cluster state, composed by the emergent structure of photon-number correlations between pairs of modes. As such, we define the correlation matrix \mathbb{C} :

$$[\mathbb{C}]_{ij} = \frac{|\langle \hat{n}_i \hat{n}_j \rangle - \langle \hat{n}_i \rangle \langle \hat{n}_j \rangle|}{\sqrt{(\langle \hat{n}_i^2 \rangle - \langle \hat{n}_i \rangle^2) \left(\langle \hat{n}_j^2 \rangle - \langle \hat{n}_j \rangle^2\right)}},\tag{4}$$

where we take the absolute value of the correlation, since we are purely interested in the strength of the correlation, rather than its sign. The values of $|\langle \hat{n}_i \hat{n}_j \rangle - \langle \hat{n}_i \rangle \langle \hat{n}_j \rangle|$ depend on the number of photons in the system; it may be higher for two weakly correlated nodes with very high photon numbers, than for strongly correlated nodes with very small photon numbers. Due to its conditional nature, photon subtraction locally changes the photon number in the system, thus making it impossible to genuinely compare the resulting values of $|\langle \hat{n}_i \hat{n}_j \rangle - \langle \hat{n}_i \rangle \langle \hat{n}_j \rangle|$ in the two cases. The denominator in equation (4) solves this problem by renormalizing the correlation to be confined between zero and one, where one implies that both nodes contain the same number of photons, regardless of how many photons there are.

Equation (4) ultimately allows us to look at the correlation network, as given by its weighted adjacency matrix:

$$\mathbb{A} = \mathbb{C} - \mathbb{1}. \tag{5}$$

In the following we will characterize what kind of correlation networks (\mathbb{A}) emerge, in the same spirit of mutual information networks in [44], when photon-subtraction operations are applied on cluster states with different shapes \mathcal{A} .

2.6. Complex network measures in complex network models

Quantitative measures of network structures have been introduced by network theory [35, 36]. From the adjacency matrix components we can calculate the degree D_i for each node i, i.e. the number of links connected to it, as

$$D_i = \sum_j \mathbb{A}_{ij}. \tag{6}$$

The degree distribution p(D) gives the probability for a randomly picked node to have the degree D. Many crucial properties of networks, like their robustness to perturbations and the spread of contamination, are determined by the functional p(D) [36].

A second quantitative measure of complexity is the local clustering coefficient. It gives information on the connections between the neighbors of a specific node, thus keeping track of local correlations around a point. A common way of defining the clustering coefficient is the number of triangles to which the node belongs divided by the number of triplets. It can be recovered from \mathbb{A} as

$$Cl_i = \frac{\sum_{j \neq k} \mathbb{A}_{ij} \mathbb{A}_{jk} \mathbb{A}_{ki}}{\sum_{j \neq k} \mathbb{A}_{ij} \mathbb{A}_{ik}} \tag{7}$$

for $i \neq j \neq k$.

Here we briefly review some of the paradigmatic models that have been proposed for real-world networks: the random network model called Erdős–Rényi (ER), the Barabási–Albert (BA) model and the Watts–Strogatz (WS) model. The ER model builds networks by randomly connecting nodes according to a uniformly random probability $p_{\rm ER}$ for two nodes to be connected. The resulting networks exhibit a binomial distribution of links per node. The ER model is able to reproduce the typical average shortest path distances between nodes of real networks.

A second model that has been introduced to reproduce typical complexity signatures of real networks is the BA model. It describes network formation processes based on the preferential attachment model: the network grows by adding new nodes. These new nodes attach with m links to old nodes. The probability of connection is proportional to the degrees of the existing nodes, such that the highest degree nodes are the preferred ones. This model is able to reproduce the power-law distribution in the degree, and thus the existence of 'hubs', i.e. nodes with very large degree, as in real-world networks.

Finally, the WS model is able to reproduce the small-world mechanism, where any node is a short path from any other in the network. Specifically, the distance between any two nodes grows as the log of the total number of nodes. It is built by starting from a regular network in which each vertex has a fixed degree k; for instance, k = 2 would correspond to a lattice in tight binding approximation. Then nodes are rewired according to a probability p_{WS} . One interesting feature of this model is that it allows one to tune continuously from regular ($p_{WS} = 0$) to random ($p_{WS} = 1$) networks.

To achieve reasonable statistics, we consider many realisations of networks made of 100 nodes for each model. For every model we also explore different parameters. These networks are small compared to typical real-world networks, but even for this small scale the different models exhibit visibly different features. In figure 2, we show a BA network built by adding m = 2 new nodes at each step in network growth; a WS network built starting from a regular network with degree per node $k = \langle D \rangle = 2$ and rewired with a probability $p_{WS} = 0.2$; and an ER network with connection probability $p_{ER} = 0.04$. One observes clear differences between the three networks, with, for example, the emergence of easily visible hubs in the BA model, shown as large blue discs in the figure. By taking 100 network realizations for each model one observes that the resulting degree distribution, shown in figure 3, is distinct in the three cases, even if they have similar average value. In particular, the logarithmic scale shows the power-law distribution for the BA networks.

In the rest of the Articlewe will consider only the BA and WS models as the ER network shows very similar features as the WS models with high rewiring probability $p_{WS} \rightarrow 1$. With the probabilistic generation of a statistically significant number of networks for each model, it will be possible to reveal specific features, in this case quantum ones, that are determined by the structure of the network.

3. Emergent networks in complex Gaussian cluster states

In this section, we explore the emergent photon-number correlation networks for different imprinted networks before any photon subtraction. The quantum state of such networks hence exhibits Gaussian statistics of quadratures. The results of this section form a benchmark to compare with the effect of photon subtraction in sections 4 and 5.

The imprinted networks are obtained by applying C_Z gates to a set of squeezed vacuum modes according to an adjacency matrix \mathcal{A} for the BA and WS models defined in section 2.6. We then examine the emergent network with adjacency matrix \mathbb{A} . Throughout all our simulations, we fix the amount of squeezing to 15dB (i.e. $s \approx 31.6$ units of shot noise) for each squeezed vacuum mode.

As described in section 2.3, the correlation between quadratures of different modes goes beyond the graphical structure imprinted by the C_Z gates, as they appear between nearest neighbours but also between next-nearest-neighbors. We then expect photon number correlations to inherit the same behaviour.

The calculation of photon number correlations for the cluster before photon subtraction can be carried out analytically by using the techniques of appendix A. We obtain the weighted adjacency matrix (as derived in appendix A.2)

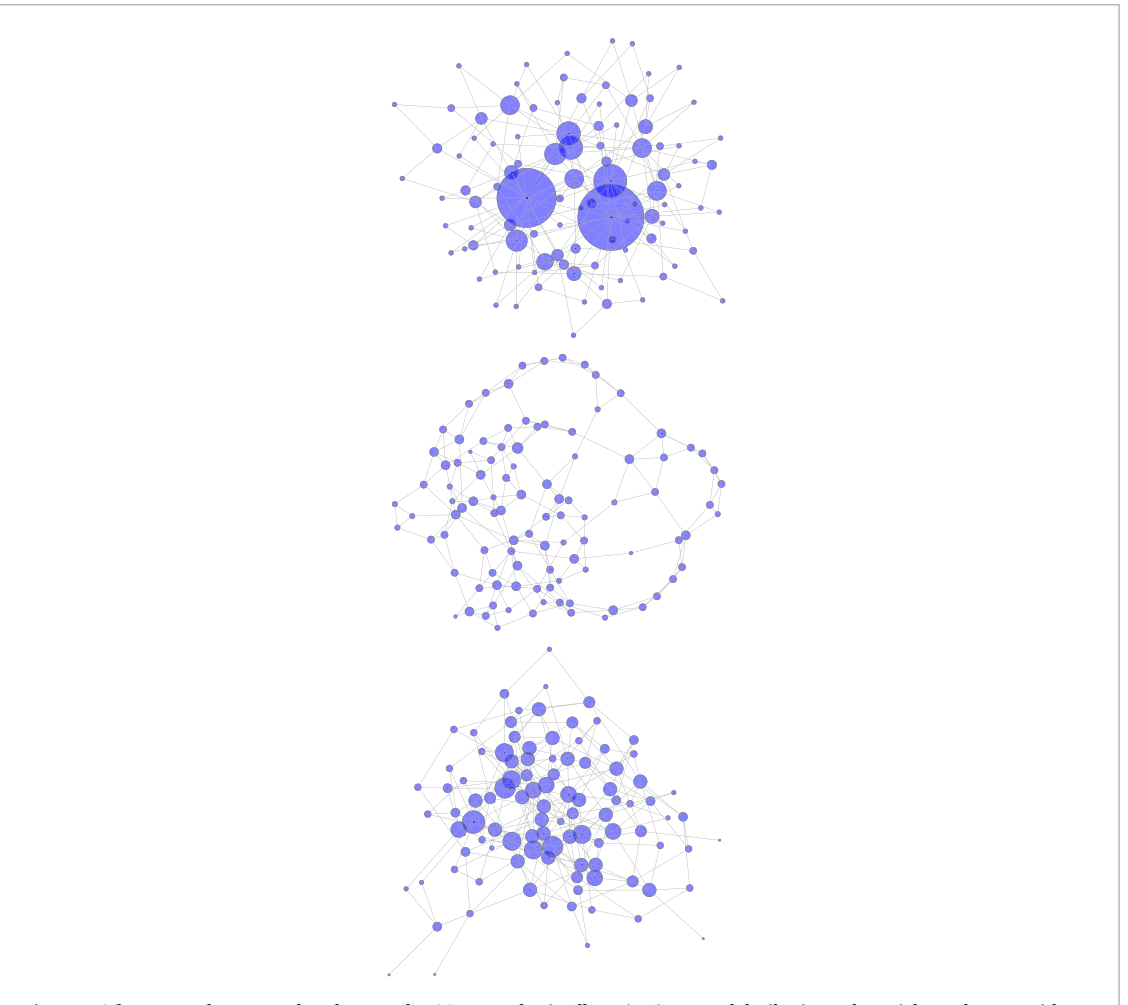


Figure 2. Three complex networks of 100 nodes. Top: Barabási–Albert (BA) network built via preferential attachment with m = 2 nodes added at each step. Middle: Watts–Strogatz (WS) network built via rewiring, with probability $p_{WS} = 0.2$, a regular network with degree per node d = 2. Bottom: Erdos–Renyi (ER) network with connection probability $p_{ER} = 0.04$. The size of the nodes is proportional to their degree.

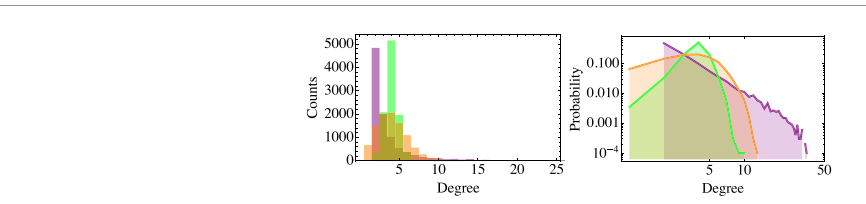


Figure 3. Histogram of the degree distribution for 100 networks of the three types shown in figure 2, BA (purple), WS (green), ER (orange). On the left the linear scale is used while on the right the scale is double-logarithmic to emphasize the appearance of the power-law tail for the BA networks. The average degree is $\langle \mathcal{D} \rangle = 4.44$ (BA), 4.0 (WS) and 4.09 (ER).

$$[\mathbb{A}]_{ij}^{G} = \begin{cases} \frac{\frac{s^{2}}{8}(([\mathcal{A}^{2}]_{ij})^{2} + 2\mathcal{A}_{ij})}{\sqrt{\mathfrak{N}(s,\mathcal{D}_{i})\mathfrak{N}(s,\mathcal{D}_{j})}}, & \text{for } i \neq j\\ 0 & \text{for } i = j \end{cases}$$
(8)

where $\mathfrak{N}(s, \mathcal{D}_k) = (s^2 + 1/s^2 + s^2(\mathcal{D}_k)^2 + 2\mathcal{D}_k - 2)/8$ is a normalization factor depending only on the initial squeezing value s and the degree \mathcal{D}_k of the node k in the imprinted network. Recall from section 2.3 that $[\mathcal{A}^2]_{ij}$ is the number of different walks of exactly two steps that connect nodes i and j in the imprinted structure. Therefore, as anticipated, the links between nodes i and j in the emergent network are non-zero if either i and j are connected in the imprinted network $(\mathcal{A}_{ij} = 1)$ or when they are next-nearest neighbors $([\mathcal{A}^2]_{ij} \neq 0)$.

So emergent networks of photon-number correlations have larger number of links than the imprinted networks. Also, the number of walks of distance two between different nodes in complex networks are larger than in regular structures (like grid shapes). Hence we expect to have a larger number of links for emergent networks of cluster with complex imprinted network.

We now look at specific features dependent on the different network structures.

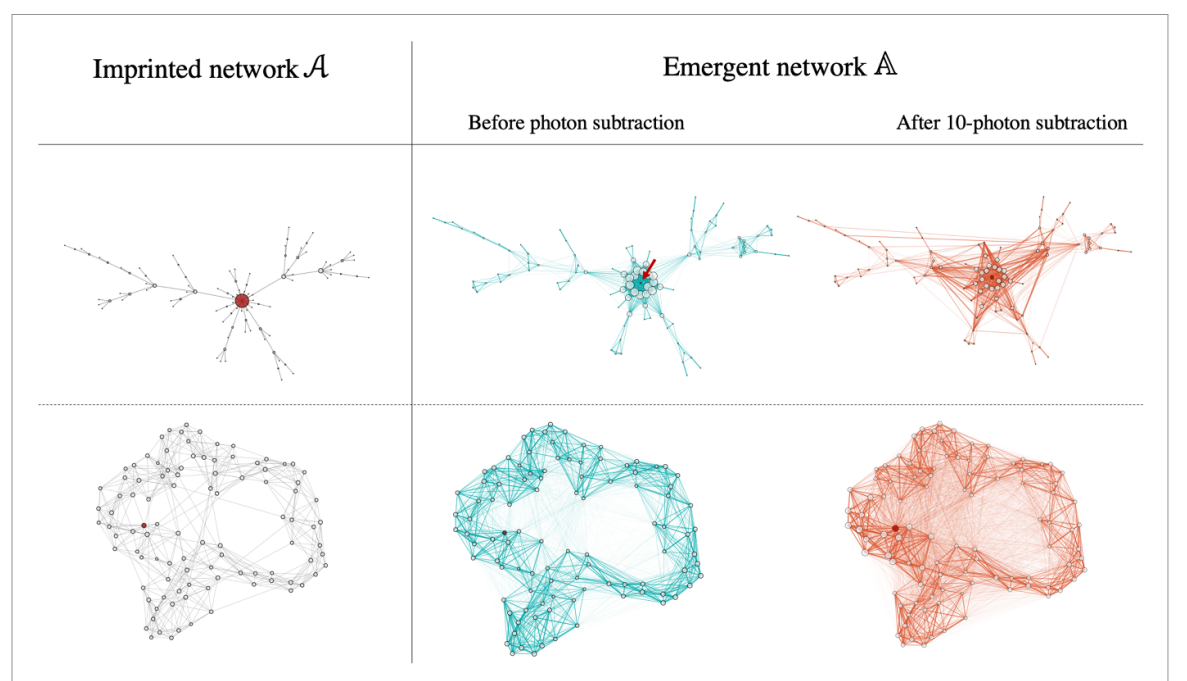


Figure 4. Imprinted networks \mathcal{A} (left column) give rise to emergent networks \mathbb{A} (middle column), which can then further undergo photon subtraction (right column). Photon subtraction at indicated red node; node sizes show the degree. Imprinted networks include Barabási–Albert with m=1 (top row) and Watts–Strogatz generated from a regular one-dimensional network in which every node is connected to its k=5 nearest neighbors with a rewiring probability $p_{WS}=0.05$ (bottom row).

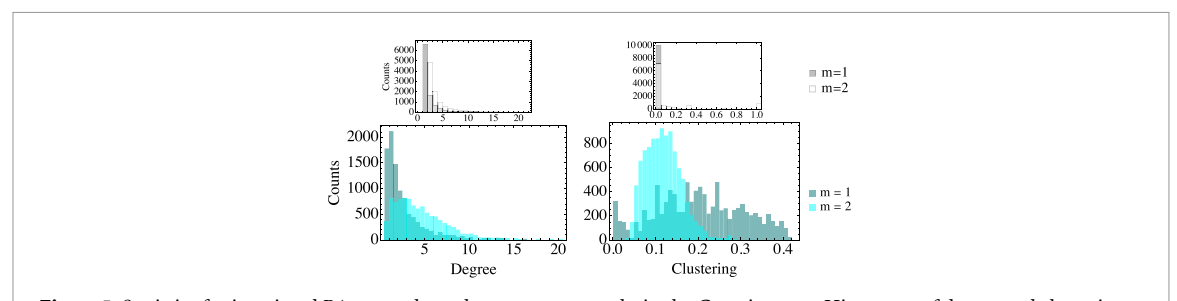


Figure 5. Statistics for imprinted BA networks and emergent networks in the Gaussian case. Histogram of degree and clustering for the imprinted BA network with m = 1 and m = 2 (top row) and associated emergent network of photon number correlations (bottom row) in the Gaussian case, i.e. when no photon is subtracted.

3.1. Barabási-Albert networks-emergent triangles and clustering

The imprinted BA networks have a multitude of weakly connected nodes that are organized around a few highly connected hubs. We collect statistics of 100 different networks of 100 nodes both for the parameter m=1 (e.g. top row of figure 4) and for m=2. In the example in figure 4, we see that the number of links in the emergent network are larger when compared to the imprinted network, as told above. A more quantitative understanding is acquired from the histograms of the degree and clustering coefficients in the emergent network of figure 5 for m=1,2 in comparison with the original distribution of the imprinted network. The emergent degree distributions inherit the features of the imprinted network, with a small number of nodes with high degrees, although with larger variances. In contrast, the histogram of clustering is dissimilar to the clustering in the imprinted network. The BA network with m=1 is an excellent example to illustrate the difference: this imprinted network's tree-like structure combined with the randomness of the BA growth process makes that many nodes have only one connection. In the emergent network, however, all nodes have at least two connections due to what we discussed above, i.e. the presence of walks at distances two in the imprinted network. So we have more triangles than in the imprinted network. Thus clustering is zero for all nodes in the imprinted network while the emergent correlation network has non-zero values quite uniformly distributed but only in the range of 0.0–0.4.

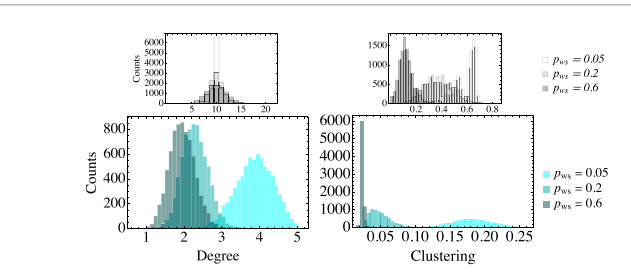


Figure 6. Statistics for imprinted WS networks and emergent networks in the Gaussian case. Histogram for the degree and clustering for the imprinted networks (top row) and for the emergent network of photon number correlations in the Gaussian case (when no photon is subtracted) (bottom row). Here results on the WS network model with $p_{WS} = 0.05, 0.2$ and 0.6 are reported.

3.2. Watts-Strogatz networks-more randomness for lower degree and clustering

For various choices of rewiring probability p_{WS} , we implemented 100 WS networks as imprinted structures to apply C_Z gates⁶. As for the BA case we look at the statistics of degree and clustering.

The bottom row of networks in figure 4 shows a typical realization of a WS network with k = 5 and $p_{WS} = 0.05$. The imprinted network is therefore reasonably close to a regular network in which each node has 2k = 10 connections. We observe that the emergent network before photon subtraction, with a weighted adjacency matrix \mathbb{A} , has a richer structure in its connections. Nevertheless, we can still see a qualitative resemblance between the imprinted and the emergent network.

In figure 6 we examine the difference in degree and clustering coefficient between imprinted and emergent networks. We observe that the properties of the imprinted WS networks strongly influence the structure of the emergent correlation networks. The degree distribution for the imprinted networks is always centered around 2k = 10 with larger variances for larger p_{WS} . The degree distributions for the emergent networks are centered around different mean values for the three p_{WS} cases. The $p_{WS} = 0.05$ case shows a broader and more skewed distribution of significantly higher degrees. Hence, for the emergent networks, in contrast to the imprinted ones, the largest variance is for the lowest p_{WS} . In general, we conclude that an increased probability of rewiring (and thus more randomness) in the imprinted network decreases the degree (which is essentially the total amount of correlation of every node) in the correlation network of Gaussian clusters. The histogram for the clustering coefficient is qualitatively similar to that of the degree, in the sense that increased rewiring leads to a decrease in clustering, and it is also very similar to the clustering of the imprinted networks⁷.

4. The effect of non-Gaussian operations on emergent networks

In this section we study the effect of photon subtraction, introduced in section 2.4, on the emergent network of photon-number correlations. Previous results show that repeated photon subtraction in the same node may increase correlations in the system due to entanglement distillation [78]. Also we know that photon subtraction in a given node creates correlations between previously uncorrelated nodes [69]. However, there is no general result on how the structure of the correlation in the network is influenced by the topology of the imprinted network.

To address this question, we monitor the effect of subtracting ten photons for the emergent photon-correlation networks. Our procedure is the following: (i) we first provide analytical results on the reach of the effect of photon subtraction. (ii) We then compare the qualitative features that are seen in the histograms of numerically generated distributions of degrees and clustering coefficients. (iii) To get a complementary quantitative view, we perform a moment analysis and probe the effect of the non-Gaussian operation on the mean, variance, skewness, and kurtosis. Readers unfamiliar with these quantities can find their definitions in appendix C. The results of this section will guide the analysis of distance -induced structures in the follwing section 5. An overview of the path followed in our network analysis can be found in figure 7. In the remainder of the Article we will explain each one of these steps in detail.

The number of photons to be subtracted (ten) is chosen in order to to have a large effect on the emergent network, although we do not find qualitatively different results for somewhat larger or smaller numbers of subtracted photons. However, increasing the amount of squeezing in the initial imprinted network or the number of photon subtractions does quantitatively enhance the observed features.

⁶ The case where $p_{WS} = 0.05$ forms an exception. Here we consider 74 realizations.

 $^{^{7}}$ While the numerator in equation (8) increases with p_{WS} , the denominator also increases in such a way that the overall C decreases. This is related to the choice of the normalization as explained in section 2.5.

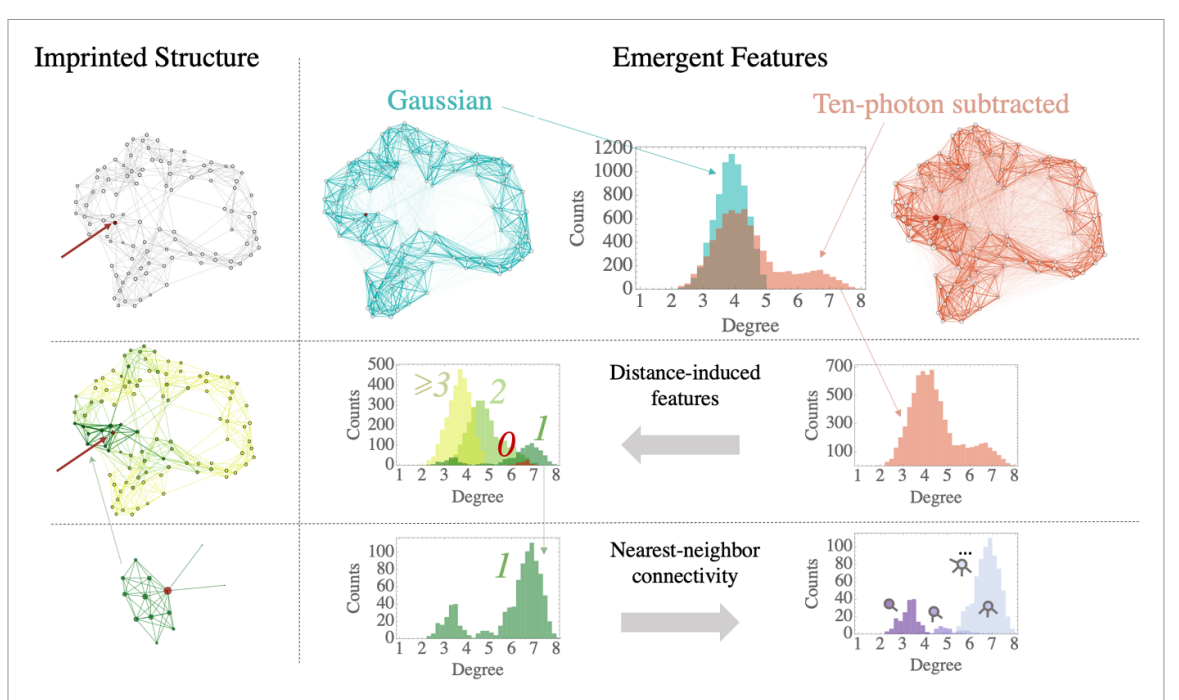


Figure 7. Analysis and structures for an imprinted WS network. Generated from a regular one-dimensional network in which every node is connected to its k = 5 nearest neighbors with a rewiring probability $p_{WS} = 0.05$. Top row: imprinted complex network (left, node with highest degree is highlighted in red); and emergent networks before subtraction (Gaussian, middle) and after subtraction (Ten-photon subtracted, right) with their corresponding degree distributions. Middle row: degree distribution of the photon-subtracted case (zoom on right) is broken up, in the central panel, according to the distance $(0, 1, 2, \text{ or } \ge 3)$ of nodes from the subtraction node. The color code used for different distances is adopted for the nodes in the imprinted network (left). Lower row: Structure of the next-neighbor nodes (distance 1) is highlighted (left); zoom of the degree distribution at distance one (middle); statistics is broken up according to the connectivity of the different nodes (right).

4.1. The effect of photon subtraction is strictly local

The subtraction of a single photon in a cluster state is known to only affect vertices in the vicinity of the node of subtraction [34]. In appendix B, we extend this understanding to the correlations between observables that are defined on different regions of the system: the correlation $\langle \hat{X}\hat{Y}\rangle - \langle \hat{X}\rangle \langle \hat{Y}\rangle$ between two observables \hat{X} and \hat{Y} can only be influenced by photon subtraction when both observables have a support on modes that are correlated to the mode of photon subtraction. This result applies regardless of the number of photons that are subtracted.

For the networks in this work, we subtract photons in one specific node. In the initial Gaussian state, equation (2) shows that this node is correlated to all nodes that are either nearest-neighbours (given by A) or next-to-nearest neighbours (given by A^2) in the imprinted network of C_Z gates. We label S the node of photon subtraction and introduce d(i,j) as the graph distance between node i and j, which counts the number of links in the imprinted network that separate the nodes.

Before photon subtraction, we show from equation (8) that $[\mathbb{C}]_{ij}$ is zero when d(i,j) > 2. Our general result of appendix B then shows that in equation (4) the numerator is affected by photon subtraction if $d(i,S) \le 2$ and $d(j,S) \le 2$. Meanwhile, the denominator is affected by photon subtraction if $d(i,S) \le 2$ or $d(j,S) \le 2$. Combining these arguments, we find that C_{ij} is affected by photon subtraction if $d(i,S) \le 2$ and $d(i,j) \le 2$, i.e. j can be up to four steps away from S.

We therefore have proven that effects of photon subtraction in such a multimode system can only affect a certain environment around the node of subtraction. Moreover, the number of nodes, in which the effect of photon subtraction is felt, is independent of the number of subtracted photons. Hence, to study the effect of photon subtraction, we can restrict ourselves to intermediate network sizes, that have a large fraction of the nodes that lie in the vicinity of the photon-subtracted node.

Figures 8 and 9 show how the size of these neighborhoods increases with the size of the network. In almost all cases we consider, we find that the size of the neighborhood grows much more slowly than the number of nodes once we surpass ~ 100 nodes (note that the horizontal axis is a logarithmic scale). The notable exception is the case of BA networks when we subtract a photon in the most highly connected node. This observation is consistent with the fact that BA networks can have very high connectivities, as is also shown by the power-law statistics in figure 3.

Note that for WS networks the size of the vicinity of the photon-subtracted node could also be changed by increasing or decreasing the connectivity k of the initial regular network that is rewired. However,

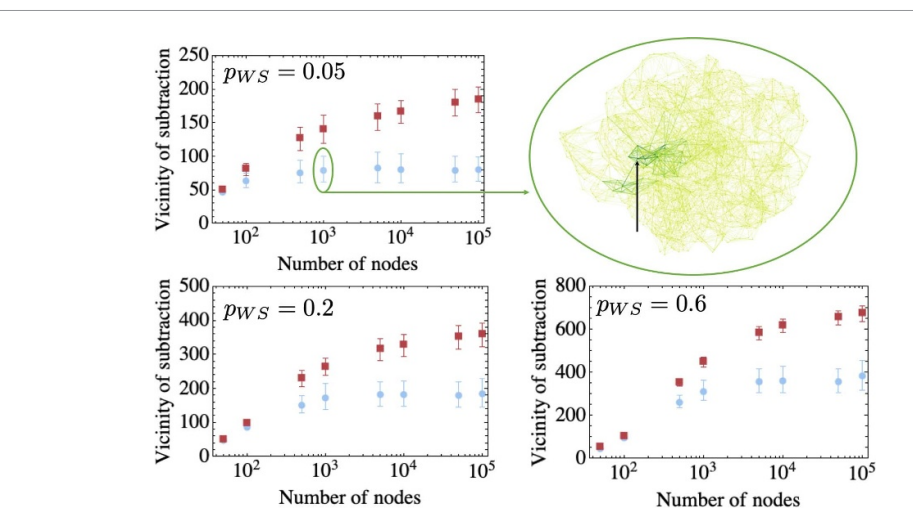


Figure 8. The nearest and next-to-nearest neighbours of the photon-subtracted node in imprinted WS network are counted and represented as the *vicinity of subtraction*. The number of nodes in this vicinity is shown as a function of the total number of nodes in the network. Every point shows the average of 100 realizations of the network, and the error bar shows the standard deviation around the average. The WS networks are generated from a regular one-dimensional network in which every node is connected to its k=5 nearest neighbors with a varying rewiring probability $p_{WS}=0.05$, $p_{WS}=0.2$, and $p_{WS}=0.6$ for the different figures. Each plot shows two possible scenarios: one where the photon is subtracted in a random node (light blue) and one where it is subtracted in the node with the highest connectivity (dark red). Finally, we also show one explicit example of a distance-resolved imprinted network of 1000 nodes, with the vicinity of the photon-subtracted node highlighted in darker green.

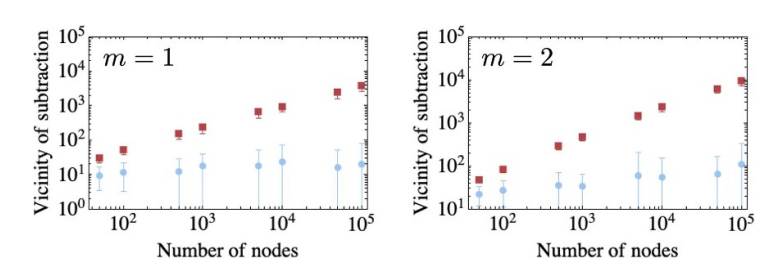


Figure 9. The nearest and next-to-nearest neighbours of the photon-subtracted node in imprinted BA network are counted and represented as the *vicinity of subtraction*. The number of nodes in this vicinity is shown as a function of the total number of nodes in the network. Every point shows the average of 100 realizations of the network, and the error bar shows the standard deviation around the average. The BA networks are generated for parameters m = 1 and m = 2 in the different panels. Each plot shows two possible scenarios: one where the photon is subtracted in a random node (light blue), and one where it is subtracted in the node with the highest connectivity (dark red).

throughout our text we choose to keep it constant at k = 5. As such, for the types of networks and the parameter ranges we consider a choice of ~ 100 nodes guarantees that most correlations in the system are affected by photon subtraction in a single node.

We also arrive at another important conclusion: to induce non-Gaussian effects in vast cluster states, one must subtract photons in many different nodes. However, in appendix A.3, we argue how the complexity of this problem effectively makes it computationally hard to simulate. From a physical point of view, one would subtract these photons by coupling a tiny amount of light from the subtracting nodes, into an auxiliary mode. Then we need photon detectors on these auxiliary modes to fire at the same time. We can notice the connections to Gaussian boson sampling [15, 17], where it is shown that simulating the clicks of photon detectors mounted on a sufficiently complicated Gaussian states is computationally intractable. Similarly, there is also a direct connection to the hardness of sampling continuous variables on a photon subtracted state [14].

On a mathematical level, the problem at the basis of the computational complexity of these sampling problems is finding perfect matchings [79]. As we argue in detail in appendix A.3, the problem of finding all perfect matchings also appears when constructing the emergent network of photon-number correlations. Hence, fully simulating such networks in detail is only possible when many photons are subtracted in many modes.

Yet, when large states with photons subtracted in various modes are created in experiments, the measurement and analysis of emergent correlation networks may well turn out to be an important tool to

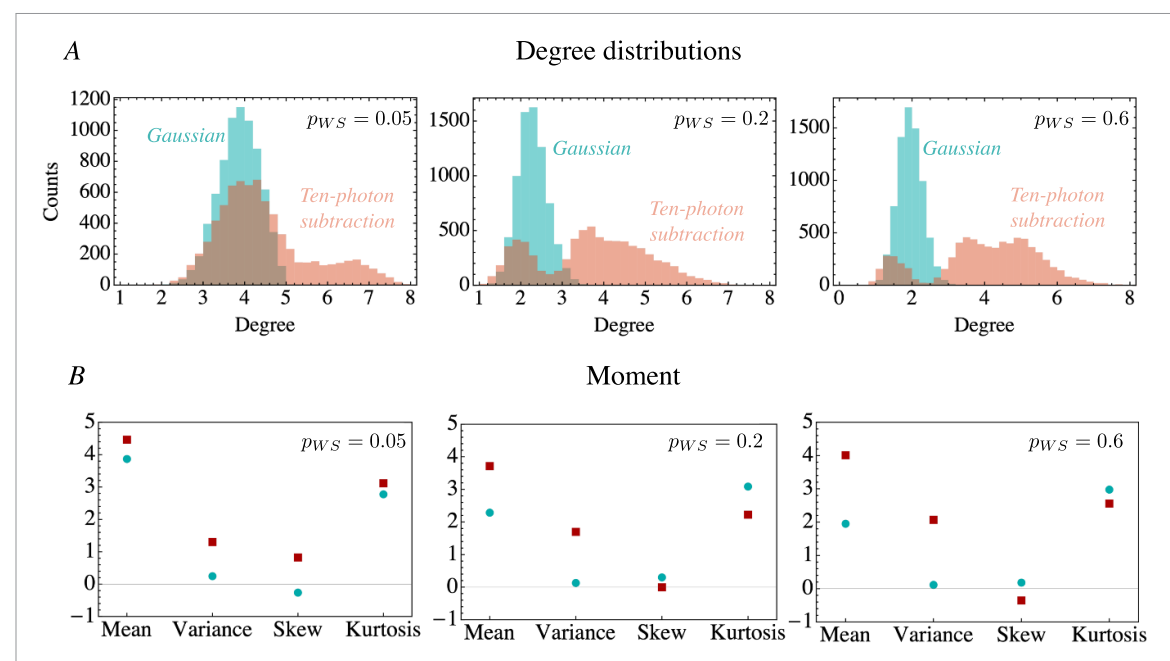


Figure 10. Histograms (A) and moments (B) for the degree distributions of the emergent correlation network obtained from a WS imprinted structure with rewiring probabilities $p_{WS} = 0.05, 0.2$ and 0.6. Colors indicate degree data prior to (cyan, dots) and after (red, squares) the subtraction of ten photons in the node with the highest connectivity. Data were each obtained by combining 74 random realizations of a 100-node network. The WS imprinted network is obtained by starting from a one-dimensional regular network where each node is connected to its k = 5 nearest neighbors. Both moments and histograms show how photon subtraction changes the bulk of the distribution by increasing the mean degree and the width of the distribution (i.e. variance). The higher moments and histograms also show that the finer structure in the tails of the degree distribution depends strongly on the value of p_{WS} .

characterise such states. Note that the same type of photon-number correlations have been used to benchmark computationally intractable Gaussian boson sampling experiments [18, 19].

4.2. Photon subtraction in Watts-Strogatz networks-more randomness for larger effects

Figure 8 suggests that we can maximize the effect of photon subtraction by subtracting the photons in the node with the highest connectivity in the imprinted network, i.e. the biggest hub. As such we probe network environments in the imprinted WS structure with the highest correlations. For the considered network size of 100 nodes, this choice has a small effect in the case of WS networks as most nodes have a similar connectivity, unlike BA networks where a few nodes serve as highly connected hubs.

In figure 10 we choose rewiring probabilities $p_{WS} = 0.05, 0.2, 0.6$, as for the Gaussian case, to probe the effect of different imprinted network environments on the degree distribution in the emergent network of photon-number correlations. The data for each value of p_{WS} are obtained by combining 74 random realizations of a 100-node network. The effect of photon subtraction is qualitatively similar in all cases. A subset of nodes in the photon-subtracted cluster states retains degrees of the same order of magnitude as for the Gaussian network state, whereas a second subset finds its degree considerably increased, resulting in a bimodal distribution. This qualitative similarity translates to the moments in figure 10(B), in the sense that photon subtraction shifts the distributions to higher means and variances, regardless of the value of p_{WS} . However, photon subtraction causes stronger increases in the mean and variance for larger values of p_{WS} , and the higher moments behave differently depending on p_{WS} . These features are observed in figure 10, where an increase in p_{WS} lowers the overlaps between the histogram before and after photon subtraction.

In figure 11, we explore the role of photon subtraction on the clustering coefficients. The observed difference between different values of p_{WS} is even more profound: the clustering coefficients are only weakly affected by photon subtraction for $p_{WS} = 0.05$, whereas for $p_{WS} = 0.6$ the histogram changes dramatically. These drastic changes are also seen when comparing the moments before and after photon subtraction in figure 11(B), where photon subtraction increases the skewness and kurtosis for $p_{WS} = 0.05$, but strongly decreases these moments for $p_{WS} = 0.6$. Nevertheless, even though the clustering coefficients are not strongly affected by photon subtraction in imprinted WS structures with $p_{WS} = 0.05$, these clustering coefficients remain much higher than those of the imprinted networks with higher values of p_{WS} (which one can also confirm in the moments).

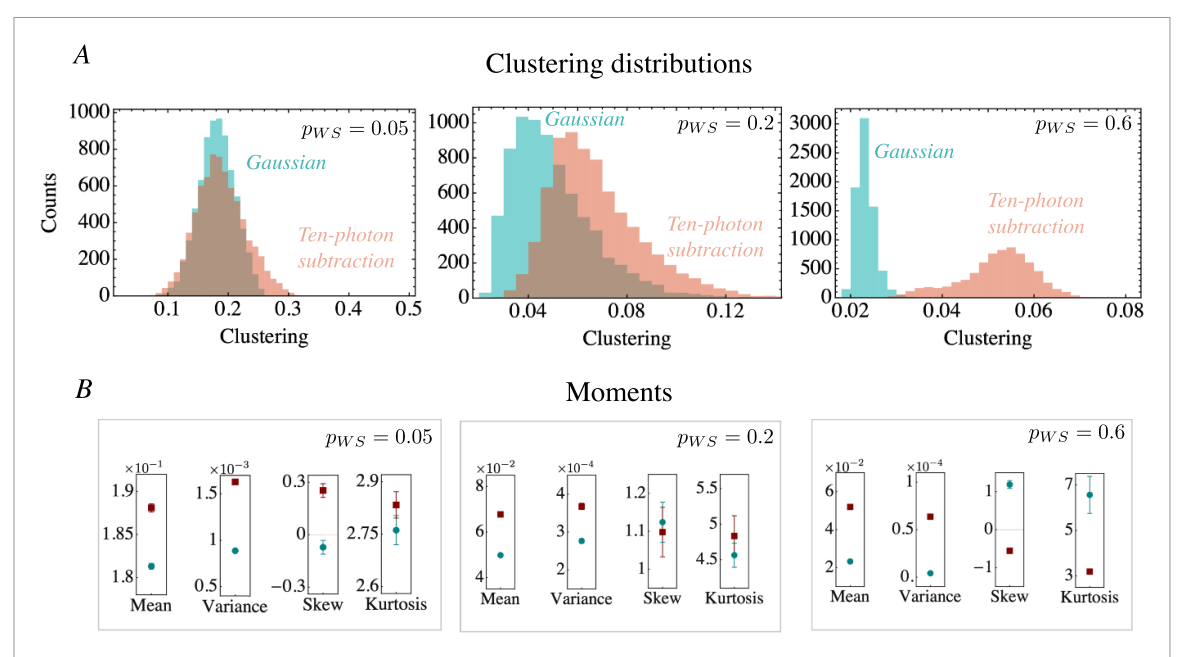


Figure 11. Histograms (A) and moments (B) for the clustering distributions for the same networks as figure 10. Colors indicate degree data prior to (cyan, dots) and after (red, squares) the subtraction of ten photons in the node with the highest connectivity. Photon subtraction shifts and widens the distribution, as shown by the histograms and quantified by the mean and variance. The higher moments and histograms indicate that the finer structure of these distributions depend strongly on the value of p_{WS} .

These observations coincide with the intuition that photon subtraction generally increases the correlations in our system. However, it remains to understand which features of the network structure associated with the different values of p_{WS} determine the extent of the effect of photon subtraction.

4.3. Photon subtraction in Barabási–Albert networks—difference between random and highly connected subtraction node

We now explore how photon subtraction affects the emergent network of a BA imprinted structure, both when we subtract always from the most important hub (i.e. the node with the highest connectivity in the imprinted network), and when we subtract in a randomly chosen node (likely a node with low connectivity).

Even before photon subtraction the moment analysis in figure 12(B) shows that for imprinted BA structures the degree distributions of emergent correlation networks have a large variance and kurtosis, in particular for m = 1. Hence, the emergent networks inherit some of the power-law features of the imprinted structures. In the top panels of figure 12 we therefore show the degree distribution on a log-log scale, for m = 1 and m = 2, before and after subtraction of ten photons.

For m=1 imprinted structures, the effect of photon subtraction manifests within the tail of the distribution. We observe the power-law behaviour that is suggested by the moments, and we find that photon subtraction in a hub tends to reduce the weight in the tail. Thus, photon subtraction in the most important hub has a reasonably small effect on a large fraction of the network to make the degrees somewhat more homogeneous. In contrast, photon subtraction increases the weight in the tail if it occurs in a randomly picked node. This shows that, when the photons are subtracted in a node that is correlated to only a small number of other nodes, it can very significantly increase these correlations, thus causing larger values to appear in the tails. This behaviour is consistent with photon subtraction as a finite resource for entanglement distillation. Yet, it must be stressed that photon-number correlation are not necessarily quantum correlations. For nodes with a high connectivity, photon subtraction only weakly alters the individual correlations. As a final comment for the m=1 case, we must note that the bulk of the distribution remains largely unaffected, up to a point where the effect of photon subtraction is hardly visible when the histogram is plotted on a linear scale—this is also reflected by a relatively small change in the mean degree.

For m=2 imprinted structures, the distribution does not show typical power-law behaviour, which is reflected in smaller values of kurtosis in figure 12(B). These moments, nevertheless, show a profound change in the variance due to photon subtraction, which implies an overall widening of the distribution. Figure 12(A) shows this feature, as now a larger fraction of the distribution grows to higher values of the degree. Hence, for m=2 we can conclude that photon subtraction predominantly affects the bulk of the distribution, which is qualitatively similar to what we saw for WS distributions.

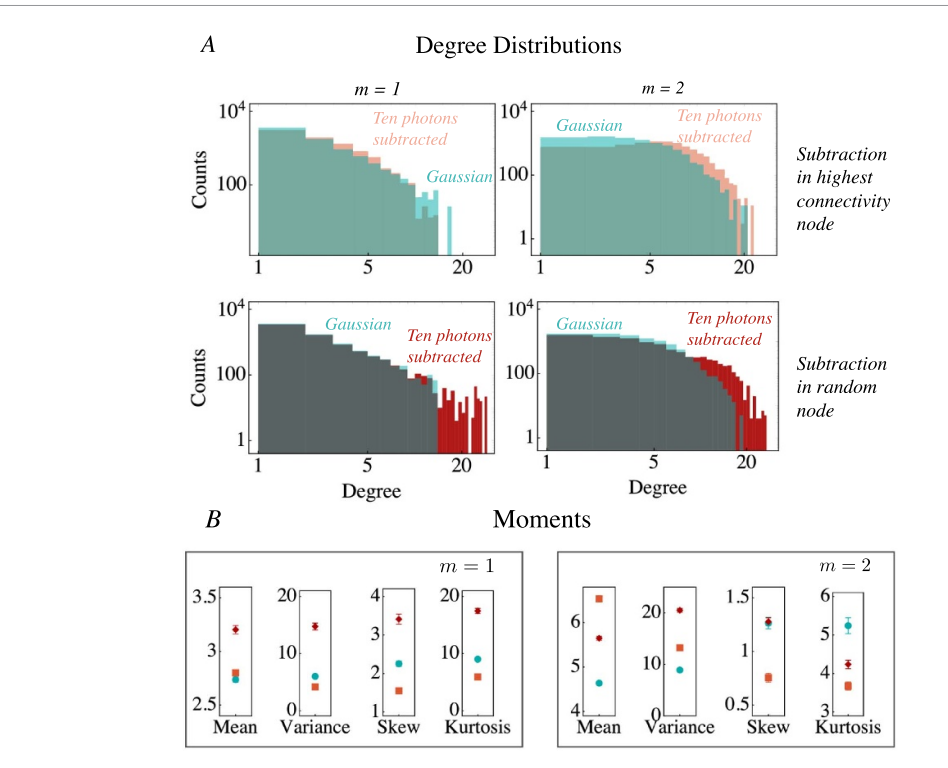


Figure 12. Logarithmically-scaled histograms (A) and moments (B) for the degree distributions of the emergent correlation network obtained from a BA imprinted structure for networks generated with m=1,2. Colors indicate degree data prior to (cyan, dots) and after the subtraction of ten photons in the node with the highest connectivity (light red squares), or in a randomly chosen (dark red diamonds) node. These histograms were each obtained by combining 100 random realizations of a 100-node network. Photon subtraction mainly affects the tails of the distribution as seen in the histograms and reflected in the variance and kurtosis. The emergent networks for m=1 imprinted structures show power-law behaviour, which is reflected by high values of the kurtosis.

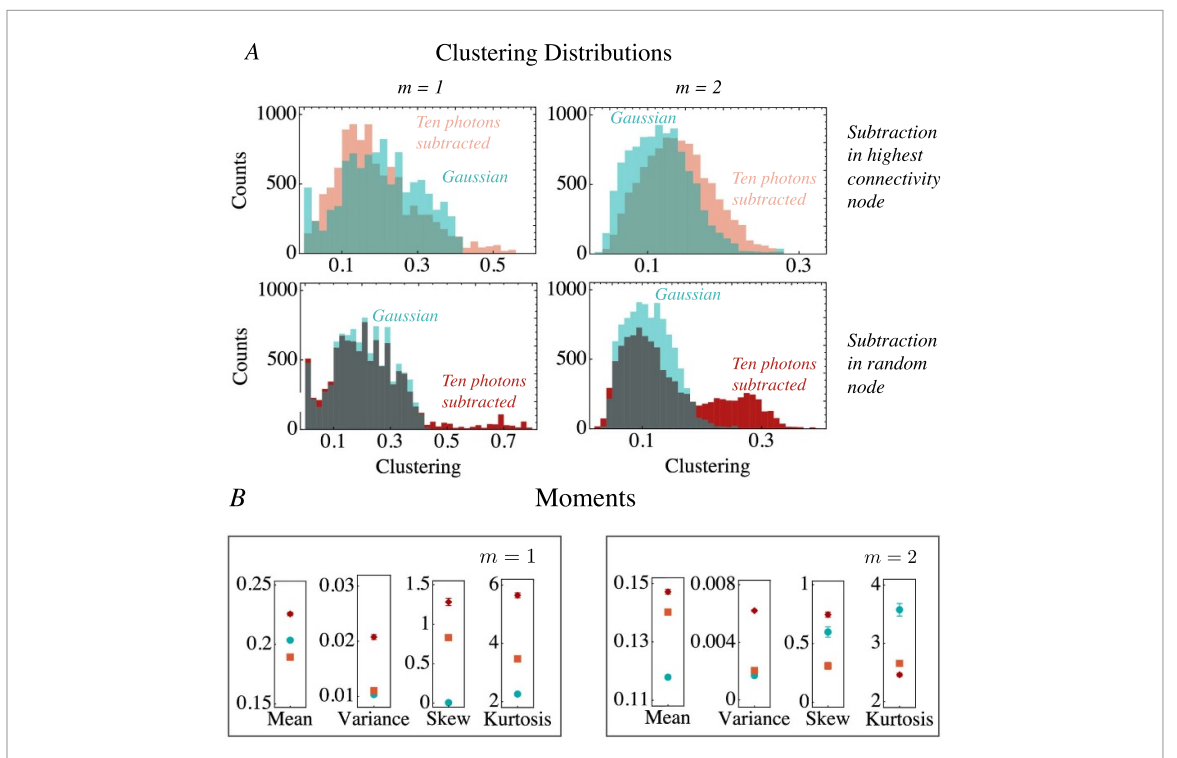


Figure 13. Histograms (A) and moments (B) for the clustering distributions of the same networks as figure 12, and the same color coding. Photon subtractions increase the tails of the distributions. Photon subtraction in a random node can create high clustering coefficients for a reasonably small number of modes.

In figure 13 we observe that for m = 1 the clustering coefficients in these networks can be increased up to Cl = 0.8, though only for a small fraction of nodes. In other words, photon subtraction, again,

predominantly affects the tails of the distribution for m=1 (which is confirmed by the moment analysis in Panel (B) of figure 13). Therefore random tree networks (i.e. BA with m=1) globally seem to be the most resilient networks to local photon subtraction operations, even though photon subtraction in nodes with few links can cause profound local changes in the correlations. For m=2 we again see a larger overall impact of photon subtraction, leading to more significant changes to the bulk of the distribution. This, too, is in line with the degree statistics.

These results suggest that the environment of the subtracted node in the imprinted network plays an important role in how the emergent network reacts to photon subtraction. To unravel this interplay between the imprinted structure and the emergent network, we will investigate the behaviour of nodes depending on their distance (in the imprinted network) to the node of photon subtraction.

Note that the power-law degree distribution of the imprinted networks can lead to very large vicinities of the photon-subtracted nodes (in particular when we subtract photons in a hub). This means that the number of non-Gaussian correlations in the networks can rapidly grow, as shown in figure 9. In our present implementation of the code to simulate the correlation networks [80], this makes BA networks beyond 100 nodes numerically very challenging to treat.

5. Imprinted structure guides non-Gaussian effects

The results in section 4.1 and the more general theorem presented in appendix B show that the study of the non-Gaussian correlations induced by photon subtraction is actually a study of sub-networks rather than the study of the global state. In this section we go beyond the simple separation of affected (i.e. the vicinity of the photon-subtracted node) and unaffected nodes, and explore more detailed sub-structures of the networks.

In section 5.1, we first explore how distances for the photon-subtracted node in the imprinted network have an effect on the emergent correlations. This will notably highlight a different behaviour for nearest and next-to-nearest neighbours. In section 5.2, we will then explore in detail how the structure of nearest-neighbour sub-networks of the imprinted networks have a profound influence on the non-Gaussian effects that manifest in the photon-number correlations.

5.1. Distance-induced structure

In section 4, we showed that photon subtraction induces additional structure in the emergent network. Here, we take the first step toward understanding how the emergent structure in photon-number correlations is influenced by the imprinted structure. We break up the statistics according to the imprinted distance between the node in which the photons were subtracted and the nodes under consideration. This distance between nodes is here understood to be the number of connections in the shortest path that connects the nodes in the imprinted structure.

In section 4.1 we emphasised that the quantity $\langle \hat{n}_i \hat{n}_j \rangle - \langle \hat{n}_i \rangle \langle \hat{n}_j \rangle$ is only altered by photon subtraction when nodes i and j are both in the vicinity of the point of photon subtraction. When at least one of the vertices lies beyond, the features of its emergent correlations are only impacted via the denominator in equation (4). For the degree statistics, this means that nodes at distances zero (point of subtraction), one (nearest neighbours), and two (next-to-nearest neighbours) are very differently affected by photon subtraction than the remaining nodes. This motivates the choice to separate the nodes into four groups: the nodes where the photons are subtracted (distance 0); their nearest neighbors (distance 1); the next-nearest neighbors (distance 2); and all the remaining nodes (distance 3 or more).

As an example of such a distance analysis, in figure 14 we show four histograms corresponding to our four chosen groups of nodes. A complementary quantitative view can be obtained by studying the moments of these distance-resolved histograms, as shown in the moments of the degree distribution in figure 15 for imprinted WS structures and in figure 16 for imprinted BA network. A completely analogous analysis can be carried out for the clustering coefficients.

The moments in figures 15 and 16 provide a range of important insights. First, we find that degree distribution of nodes that lie beyond the next-nearest neighbors (\geqslant 3) are generally unaltered by photon subtraction. A notable exception is found for the imprinted BA network with photon subtraction in a random node, where the higher moments, i.e. skewness and kurtosis, for these nodes are influenced. This is consistent with the idea that, for an imprinted BA network with photon subtraction in a random node, the non-Gaussian effects are confined to a smaller number of nodes, which in turn change more drastically.

As a second observation, we find that the distance-dependent effects in the skewness and kurtosis depend strongly on the specific network-type and chosen parameters, in contrast to the mean and variance. This implies that photon subtraction induces some general effects on the bulk of degree distributions (as

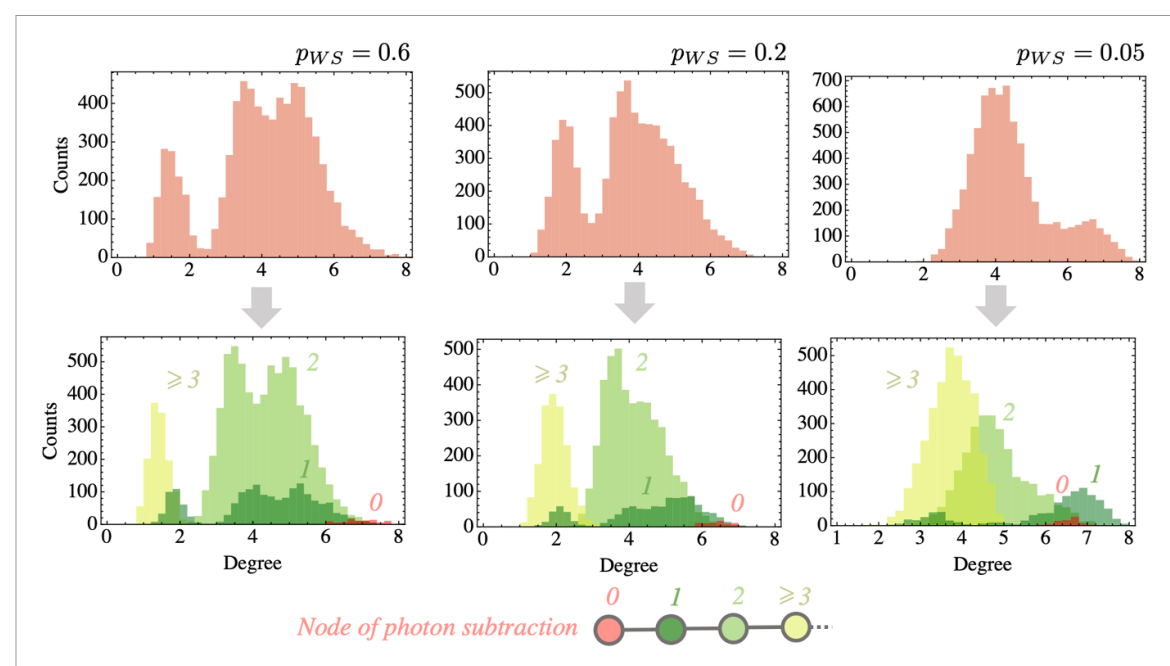


Figure 14. Degree distribution of the emergent network of imprinted WS networks after the subtraction of ten photons, using the same data as figure 10. Complete histograms (top) were each obtained by combining all the nodes of 74 random realizations of a 100-node network (see also figure 10). Distance-resolved histograms (bottom) are obtained by grouping nodes based on their network distance (in the imprinted network) to the node of photon subtraction. Network distance is indicated by color code and labeled by a number (zero being the node of subtraction). Photon subtraction shifts the degree distribution to higher values for the nodes of photon subtraction (distance 0) and those at distance 2. At distance 3 and beyond, the effects are negligible. At distance 1 the distribution is affected in a non-trivial way depending on p_{WS} . The value of p_{WS} also influences the relative importance of distance-induced features, e.g. for $p_{WS} = 0.05$ we find a larger fraction of nodes at distance 3 or beyond.

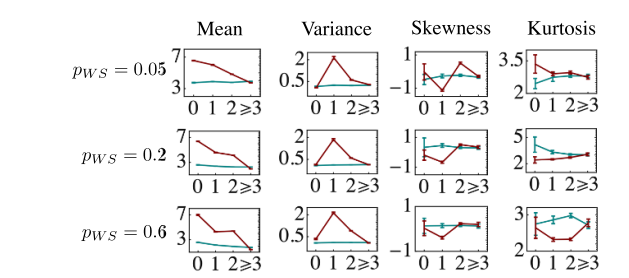


Figure 15. Distance-resolved moments for the degree statistics in the emergent photon-number correlation network, resulting from imprinted WS networks with rewiring probabilities $p_{WS} = 0.05$, $p_{WS} = 0.2$, and $p_{WS} = 0.6$. Gaussian states (cyan) and ten-photon subtracted states (red). Photon subtraction mean and variance are affected in the same way for all networks, showing that photon subtraction has the global tendency of increasing the degree and widening the distribution of nodes up to distance 2. The effect on higher moments depends on the value of p_{WS} , showing that photon subtraction also affects the fine structure of the degree distribution in a more subtle way that depends on the network topology. At distance 3 and beyond we see no effect.

comprised by the first two moments), while the effect on the finer structure (as comprised by the higher moments) of the degree distributions depends more strongly on the precise topology of the imprinted networks

As an important general effect, we find that both for the nodes in which photons are subtracted (0) and their next-nearest neighbors (2) the mean and variance of the degree distribution always increase. The behaviour of the nearest neighbors (1) is less systematic. For imprinted BA networks with photon subtraction in a random vertex, the mean and variance are essentially unaltered for the nearest neighbors. In contrast, for imprinted WS networks, and the m=2 BA network with photon subtraction in the node with highest connectivity, the mean and variance increase for these nodes. For the imprinted BA network with m=1 and photon subtraction in the node with highest connectivity, we find that the mean and variance decrease after photon subtraction. Hence, there must be other features in the topology of the imprinted network that influence the degree distribution of the nearest neighbors. These features will be laid out in the following subsection.

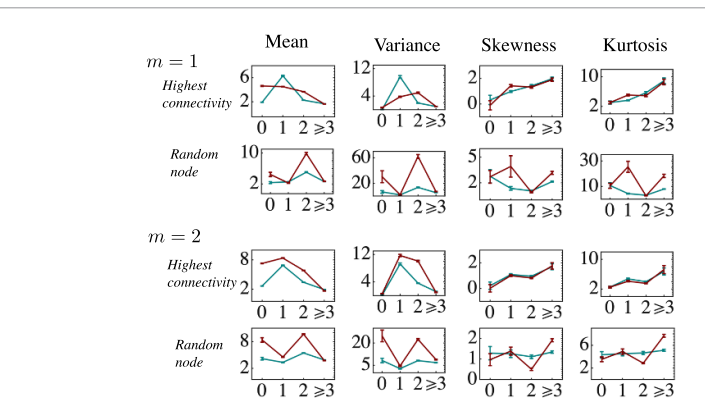


Figure 16. Distance-resolved moments for the degree statistics in the emergent photon-number correlation network, resulting from imprinted BA networks with parameters m = 1 and m = 2. Gaussian states (cyan) and ten-photon subtracted states (red). The same observations hold as for the WS networks in figure 15, except for the distance 1 nodes in imprinted structures with m = 1. The latter is explained in detail in section 5.2.

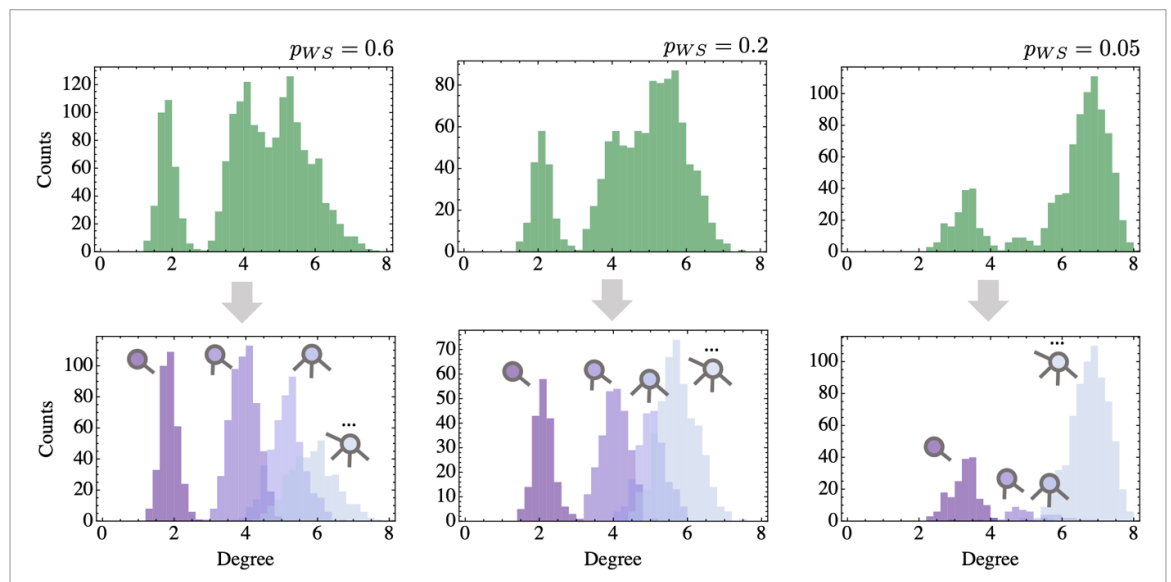


Figure 17. Nearest-neighbor (1) degree distribution of the emergent network after the subtraction of ten photons, using the same data as figure 14. Top row: complete nearest-neighbor histograms. Bottom row: histograms obtained by grouping nearest-neighbor nodes based on the number of other nearest-neighbor nodes they are connected to in the nearest-neighbour subnetwork. The connectivity in the nearest-neighbor sub-network is highlighted by the nodes represented next to the histogram. Nearest neighbors of the node of photon subtraction are more strongly affected by the non-Gaussian operation when they are connected to other nearest neighbors. Nodes that are not connected to any other nearest neighbors (darkest purple) are shifted to lower degrees as compared to the Gaussian distributions in figure 10.

5.2. Nearest-neighbors (1) subnetworks

In figure 17 we show that the effect on the degree of a nearest-neighbor node in the emergent correlation network is influenced by the number of other nearest neighbors it is connected to in the imprinted networks. This highlights the importance of the topology of the distance-1 sub-network, as compared to the total imprinted network. Quantitatively, this connectivity can be obtained by analyzing the nearest-neighbor sub-network. When we analyze all the nearest-neighbor sub-networks of our simulated WS networks, we obtain the result in figure 17. The bottom row of figures clearly shows that the degrees (in the emergent network) of nearest neighbors are more strongly affected by photon subtraction when these nodes have a higher number of connections to other nearest neighbors. Thus, the different shapes of the nearest neighbor distributions (1), for different values of the rewiring probability p_{WS} , can be fully understood from the nearest neighbor sub-network in the imprinted structure.

We note that photon subtraction shifts the histograms which group nearest-neighbor nodes according to their connectivity in the distance-1 sub-network to higher mean values for higher connectivity. However, for nodes that are not connected to other nearest neighbors, we witness a slight decrease in the average degree due to photon subtraction.

For $p_{WS} = 0.6$ a significant fraction of nearest neighbors are not connected to any other nearest neighbors. This provides a sharp contrast with the case for $p_{WS} = 0.05$, where networks tend to form clusters, such that nearest neighbors are more likely to be connected to each other. From figure 17, we can understand how these features of the imprinted structure have a direct effect on the statistical features of the emergent network.

Similar analyses have been carried out for the nearest neighbor networks of all simulated classes of networks, leading to the same results. A particularly striking case is the BA network with m=1: because these networks are tree-like, nearest neighbors are never connected to one another. This explains why in figure 16, for m=1, the means for nearest neighbors (1) are reduced by photon subtraction. Moreover, we can now explain why in figure 16 the contribution of the nearest-neighbor sub-network for photon subtraction from the highest degree node for BA with m=2 is more important than in the case of subtraction from a random node. In this latter case it is more likely to select one of the isolated nodes with a surrounding nearest-neighbor sub-network also characterized by low connectivity. However, the analysis is not sufficient to explain why the next-to-nearest neighbors (2) are so strongly affected by photon subtraction from a random node in the BA network with m=2.

6. Discussion and outlook

The key findings of this work were already summarised in section 1.2. These results prove that complex network methods are useful for the theoretical investigation non-Gaussian cluster states. The characterization of highly multimode non-Gaussian states is generally an arduous task, where standard tools of CV quantum optics fall short. Typical experimental methods such as homodyne tomography lack the necessary scaling properties to study these systems, and theoretical constructs such as Wigner functions become hard to handle. To overcome this problem, one may look for global properties, e.g. Wigner negativity of the full multimode states [12]. Such global features have the disadvantage that they gloss over the local or neighborhood structures of the state, which are essential in multi-partite quantum platforms. Our results show that network theory offers effective statistical tools for studying these states. At present, we are unaware of any other method that allows us to describe the physical features that we deduced for these large non-Gaussian states. They offer us a road map for more detailed bottom-up studies of particular features such as the role of connections in the nearest-neighbor sub-network.

Data availability statement

The data that support the findings of this study are openly available at the following URL/DOI: https://github.com/mwalschaers/ComplexNetworks.

Acknowledgments

This work was supported by the European Research Council under the Consolidator Grant COQCOoN (Grant No. 820079). This work was also performed in part with support by the U.S. National Science Foundation under Grants PHY-2210566 and CCF-1839232. We thank the Complex Quantum Systems group at Laboratoire Kastler Brossel (and in particular D Delande) for access to their computational facilities.

The software used to generate the complex networks in the Article is available on [80].

Appendix A. Simulating cluster states and the evaluation of photon-number correlations

A.1. Perfect matching

To execute the simulations presented in this article, we generated random complex networks using the 'python-inetwork' library. From these randomly generated networks, we extracted the adjacency matrix \mathcal{A} to generate the cluster state covariance matrices, as described in equation (2). After generating the covariance matrix V of a Gaussian network state, we used it to evaluate the photon-number correlations $[\mathbb{C}]_{ij}$ of equation (4) for the photon-subtracted states in equation (3).

The main technique used to evaluate these correlations relies on the properties of Gaussian quantum states. We previously used this method to fully characterize single-photon subtracted states in [8]. We illustrate this method by highlighting the evaluation of the element $\langle \hat{n}_i \hat{n}_j \rangle$ in equation (4). For a photon-subtracted state we find

$$\langle \hat{n}_{i} \, \hat{n}_{j} \rangle = \frac{\text{tr}[\hat{a}_{S_{n}}^{\dagger} \dots \hat{a}_{S_{1}}^{\dagger} \hat{a}_{i}^{\dagger} \, \hat{a}_{j}^{\dagger} \, \hat{a}_{j} \hat{a}_{i} \hat{a}_{S_{1}} \dots \hat{a}_{S_{n}} \rho]}{\text{tr}[\hat{a}_{S_{n}}^{\dagger} \dots \hat{a}_{S_{1}}^{\dagger} \, \hat{a}_{S_{1}} \dots \hat{a}_{S_{n}} \rho]}, \tag{A.1}$$

where ρ denotes the density matrix of the Gaussian network state and $i \neq j$. We then use a general property for Gaussian states, that allows us to express

$$\operatorname{tr}[\hat{a}_{S_n}^{\dagger} \dots \hat{a}_{S_1}^{\dagger} \hat{a}_i^{\dagger} \hat{a}_j^{\dagger} \hat{a}_j \hat{a}_i \hat{a}_{S_1} \dots \hat{a}_{S_n} \rho] = \sum_{\mathcal{P}} \prod_{\{p_1, p_2\} \in \mathcal{P}} \operatorname{tr}[\hat{a}_{p_1}^{\#} \hat{a}_{p_2}^{\#} \rho], \tag{A.2}$$

where we introduce the label \mathcal{P} to denote a 'perfect matching.' A perfect matching means any way of dividing a set up into pairs, while maintaining the order. When we consider, for example the set $\{1,2,3,4\}$, one possible perfect matching would be $\{\{1,3\},\{2,4\}\}$. In this example, the notation $\{p_1,p_2\} \in \mathcal{P}$ refers to $\{1,3\}$ and $\{2,4\}$. In equation (A.2), these perfect matchings are used to split the set of creation and annihilation operators, $\hat{a}_{S_n}^{\dagger} \dots \hat{a}_{S_n}^{\dagger} \hat{a}_i^{\dagger} \hat{a}_j^{\dagger} \hat{a}_i \hat{a}_{S_n} \dots \hat{a}_{S_n}$, in pairs: In total, we have 2n+4 creation and annihilation operators, which we can associate with a set of indices $\{1,\dots,2n+4\}$. The sum over \mathcal{P} runs over all possible perfect matchings of this index set. For every given perfect matching \mathcal{P} , we then multiply all the quantities $\text{tr}[\hat{a}_p^{\#}\hat{a}_{p_2}^{\#}\rho]$ for the different paired indices $\{p_1,p_2\} \in \mathcal{P}$. The quantities p_1 and p_2 are indices in the index set, and the quantity $\hat{a}_{p_j}^{\#}$ denotes the creation or annihilation operator that occurs at the p_j th position in the product $\hat{a}_{S_n}^{\dagger} \dots \hat{a}_{S_n}^{\dagger} \hat{a}_j^{\dagger} \hat{a}_j \hat{a}_i \hat{a}_{S_1} \dots \hat{a}_{S_n}$. Let us list some examples: $\text{tr}[\hat{a}_1^{\#}\hat{a}_2^{\#}\rho] = \text{tr}[\hat{a}_{S_1}^{\dagger}\hat{a}_{S_2}^{\dagger}\rho]$, $\text{tr}[\hat{a}_2^{\#}\hat{a}_{n+3}^{\#}\rho] = \text{tr}[\hat{a}_{S_1}^{\#}\hat{a}_{S_1}^{\#}\rho] = \text{tr}[\hat{a}_{S_1}^{\#}\hat{a}_{S_1}^{\#}\rho]$

What remains is now to evaluate the quantities $\operatorname{tr}[\hat{a}_{p_1}^{\#}\hat{a}_{p_2}^{\#}\rho]$, and this can be done directly via the covariance matrix V, by expressing the creation and annihilation operators in terms of quadrature operators (see also [8, 24] for more details). We find the following identities:

$$\operatorname{tr}[\hat{a}_{j}^{\dagger}\hat{a}_{k}^{\dagger}\rho] = \frac{1}{4}[V_{jk} - V_{j+N,k+N} - i(V_{j,k+N} + V_{j+N,k})], \tag{A.3}$$

$$tr[\hat{a}_{j}\hat{a}_{k}\rho] = \frac{1}{4}[V_{jk} - V_{j+N,k+N} + i(V_{j,k+N} + V_{j+N,k})], \tag{A.4}$$

$$\operatorname{tr}[\hat{a}_{j}^{\dagger}\hat{a}_{k}\rho] = \frac{1}{4}[V_{jk} + V_{j+N,k+N} + i(V_{j,k+N} - V_{j+N,k}) - 2\delta_{jk}]. \tag{A.5}$$

These identities are expressed in the mode basis that corresponds to the nodes of the network state.

Using equations (2) and (A.3)–(A.5), we can calculate the weighted adjacency matrix of the emergent network, \mathbb{A}_{ij} . In principle, it is possible to calculate \mathbb{A}_{ij} for both the cluster state as well as the photon-subtracted state. However, as we will show, it is exponentially difficult to write a closed-form expression for \mathbb{A}_{ij} in the photon-subtracted state. Below, we will first calculate \mathbb{A}_{ij} in the cluster state. Then we discuss the photon-subtracted case.

A.2. Gaussian state

Since the cluster state ρ is Gaussian, one can evaluate the connected correlation $c_{ij} \equiv \text{tr}[\hat{n}_i \hat{n}_j \rho] - \text{tr}[\hat{n}_i \rho] \text{tr}[\hat{n}_j \rho]$ by applying equation (A.2). Only two terms remain, giving

$$c_{ij} = \operatorname{tr}[\hat{a}_i^{\dagger} \hat{a}_j \rho] \operatorname{tr}[\hat{a}_i \hat{a}_j^{\dagger} \rho] + \operatorname{tr}[\hat{a}_i^{\dagger} \hat{a}_j^{\dagger} \rho] \operatorname{tr}[\hat{a}_i \hat{a}_j \rho]. \tag{A.6}$$

Each term on the right hand side of equation (A.6) can be evaluated using equations (2) and (A.3)–(A.5). For $i \neq j$, we have

$$\operatorname{tr}[\hat{a}_{i}^{\dagger}\hat{a}_{j}\rho] = s(\mathcal{A}^{2})_{ij}/4,$$

$$\operatorname{tr}[\hat{a}_{i}\hat{a}_{j}^{\dagger}\rho] = s(\mathcal{A}^{2})_{ij}/4,$$

$$\operatorname{tr}[\hat{a}_{i}^{\dagger}\hat{a}_{j}^{\dagger}\rho] = -(s(\mathcal{A}^{2})_{ij} - 2is\mathcal{A}_{ij})/4,$$

$$\operatorname{tr}[\hat{a}_{i}^{\dagger}\hat{a}_{j}\rho] = -(s(\mathcal{A}^{2})_{ij} + 2is\mathcal{A}_{ij})/4.$$
(A.7)

Therefore

$$c_{ij} = \frac{s^2}{8} \left((\mathcal{A}^2)_{ij}^2 + 2\mathcal{A}_{ij} \right) \tag{A.8}$$

where we used that $(A_{ij})^2 = A_{ij}$.

For i = j, we have

$$\operatorname{tr}[\hat{a}_{i}^{\dagger}\hat{a}_{i}\rho] = (s+1/s+s\mathcal{D}_{i}-2)/4,$$

$$\operatorname{tr}[\hat{a}_{i}\hat{a}_{i}^{\dagger}\rho] = (s+1/s+s\mathcal{D}_{i}+2)/4,$$

$$\operatorname{tr}[\hat{a}_{i}^{\dagger}\hat{a}_{i}^{\dagger}\rho] = (s-1/s-s\mathcal{D}_{i})/4,$$

$$\operatorname{tr}[\hat{a}_{i}\hat{a}_{i}\rho] = (s-1/s-s\mathcal{D}_{i})/4,$$

$$(A.9)$$

where we used that $A_{ii} = 0$ and $(A^2)_{ii} = D_i$. Therefore

$$c_{ii} = \frac{1}{8} \left(s^2 + \frac{1}{s^2} + s^2 (\mathcal{D}_i)^2 + 2\mathcal{D}_i - 2 \right). \tag{A.10}$$

One obtains equation (8) in the main text from equations (A.8) and (A.10), where c_{ii} is denoted in the main text as $\mathfrak{N}(s, \mathcal{D}_i)$.

A.3. Photon-subtracted states

For photon-subtracted states, the correlations quickly become hard to evaluate. At the basis of this complexity lies the appearance of perfect matchings in equation (A.2). Finding all possible perfect matchings is a computationally hard problem that belongs to the complexity class #P. It is also the problem which lies at the basis of the hardness of Gaussian Boson sampling. Hence, when the number of subtracted photons grows, correlation functions quickly become practically impossible to evaluate.

Generally speaking, the best algorithms for evaluating equation (A.2) use recursive techniques. In our work, we greatly simplify this computational problem by subtracting all the photons in the same mode, i.e. $S_1 = \cdots = S_n = S$. In this case, expression (A.1) for $\langle \hat{n}_i \hat{n}_j \rangle$ only contains creation and annihilation operators in three different modes. This greatly limits the different possible factors $\operatorname{tr}[\hat{a}_{p_1}^\# \hat{a}_{p_2}^\# \rho]$ that can appear in equation (A.2). Many different partitions will lead to equivalent contributions. The problem thus reduces to that of identifying all the different classes of partitions, evaluating the contribution, and counting the multiplicity.

Once we subtract more than three photons, the total number of different classes of terms remains fixed. We evaluated these by hand and counted a total of 43 classes, each appearing with a certain multiplicity. The correlation networks are then calculated by evaluating the contribution by multiplying relevant quantities given by equations (A.3)–(A.5) for each of these 43 classes. Then we multiply each contribution with the right multiplicity, which depends on the number of subtractions and can be calculated through combinatorics. The quantities $\langle \hat{n}_i \rangle$ are evaluated using the same method. For more details, we refer to the code that was used to carry out the simulations [80].

In appendix B, we prove analytically that the photon number correlations $\langle \hat{n}_i \hat{n}_j \rangle - \langle \hat{n}_i \rangle \langle \hat{n}_j \rangle$ only change when nodes i and j are in the vicinity of of the photon-subtracted node (see appendix B for details). This implies that we can first generate a full correlation network of Gaussian correlations by relying on the analytical formula (A.8) and subsequently we can use (A.2) to update only the affected correlations. This method is implemented in the second version of our code for simulating WS networks [80].

Appendix B. Correlations unaffected by photon subtraction

In this section of the appendix, we prove a general result for correlations in *n*-photon subtracted states: photon subtraction can only change the covariance between observables, if both observables are initially correlated to the mode in which the photons are subtracted.

Assume that we subtract n photons from Gaussian state ρ in a mode with label S and associated annihilation operator \hat{a}_S . We denote the algebra of observables $\mathcal{A}_{\text{near}}$ as those observables which are 'near to S' in the sense that $\mathcal{A}_{\text{near}}$ is generated by observables \hat{a}_k and \hat{a}_k^{\dagger} for which either $\text{tr}[\hat{a}_k^{\dagger}\hat{a}_S\rho] \neq 0$ or $\text{tr}[\hat{a}_k\hat{a}_S\rho] \neq 0$. Following equations (A.3)–(A.5) we can equivalently define $\mathcal{A}_{\text{near}}$ as the algebra of observables restricted to the modes with labels k for which the matrix

$$\begin{pmatrix} V_{Sk} & V_{Sk+N} \\ V_{S+Nk} & V_{S+Nk+N} \end{pmatrix} \neq \begin{pmatrix} 0 & 0 \\ 0 & 0 \end{pmatrix}. \tag{B.1}$$

We then define A_{far} as the complement of A_{near} in the sense that $A_{near} \otimes A_{far} = A$, where A is the full algebra of observables on the N-mode Fock space that describes the entire system.

Theorem B.1. For any observable $\hat{X} \in \mathcal{A}_{near}$ and another arbitrary observable $\hat{Y} \in \mathcal{A}_{far}$, it holds that

$$\langle \hat{X}\hat{Y}\rangle - \langle \hat{X}\rangle \langle \hat{Y}\rangle = \text{tr}[\hat{X}\hat{Y}\rho] - \text{tr}[\hat{X}\rho]\text{tr}[\hat{Y}\rho], \tag{B.2}$$

where $\langle \dots \rangle$ denotes the expectation value in the n-photon subtracted state and $tr[\dots \rho]$ is the expectation value in the initial Gaussian state.

Proof. We first of all use that every observable $\hat{X} \in \mathcal{A}_{near}$ can be arbitrarily well approximated by a polynomial in creation and annihilation operators in A_{near} . This implies that

$$\hat{X} = \sum_{j=0}^{\infty} \sum_{k} c_{j,k} \hat{a}_{1,k}^{\#} \dots \hat{a}_{j,k}^{\#}, \tag{B.3}$$

where $\hat{a}_{1,k}^{\#}$ can either be a creation or an annihilation operator. The sum over k takes into account that there are many possible products of creation and annihilation operators, also known as Wick monomials, of length j. And similarly for \hat{Y} we find

$$\hat{Y} = \sum_{j=0}^{\infty} \sum_{k} c_{j,k} \hat{b}_{1,k}^{\#} \dots \hat{b}_{j,k}^{\#}.$$
(B.4)

To highlight that the creation and annihilation operators that build \hat{X} and \hat{Y} have different supports, we have noted the the creation and annihilation operators for A_{far} as $\{b_{i,k}^{\#}\}$.

The fact that any observable can be written as a series expansion of creation and annihilation operators implies that our theorem can be proven by proving that

$$\langle \hat{a}_{1}^{\#} \dots \hat{a}_{j}^{\#} \hat{b}_{1}^{\#} \dots \hat{b}_{j'}^{\#} \rangle - \langle \hat{a}_{1}^{\#} \dots \hat{a}_{j}^{\#} \rangle \langle \hat{b}_{1}^{\#} \dots \hat{b}_{j'}^{\#} \rangle = \operatorname{tr}[\hat{a}_{1}^{\#} \dots \hat{a}_{j}^{\#} \hat{b}_{1}^{\#} \dots \hat{b}_{j'}^{\#} \rho] - \operatorname{tr}[\hat{a}_{1}^{\#} \dots \hat{a}_{j}^{\#} \rho] \operatorname{tr}[\hat{b}_{1}^{\#} \dots \hat{b}_{j'}^{\#} \rho]. \tag{B.5}$$

First of all, let us consider the term

$$\langle \hat{b}_1^{\#} \dots \hat{b}_{j'}^{\#} \rangle = \frac{\operatorname{tr}\left[\left(\hat{a}_S^{\dagger}\right)^n \hat{b}_1^{\#} \dots \hat{b}_{j'}^{\#} \left(\hat{a}_S\right)^n \rho\right]}{\operatorname{tr}\left[\left(\hat{a}_S^{\dagger}\right)^n \left(\hat{a}_S\right)^n \rho\right]}.$$
(B.6)

Because $\hat{b}_1^\#,\dots,\hat{b}_{j'}^\#\in\mathcal{A}_{\mathrm{far}}$, we find that $\mathrm{tr}[[\rho]\hat{b}_k^\dagger\hat{a}_S]=0$ and $\mathrm{tr}[[\rho]\hat{b}_k\hat{a}_S]=0$. An application of equation (A.2) than shows that

$$\operatorname{tr}\left[\left(\hat{a}_{S}^{\dagger}\right)^{n}\hat{b}_{1}^{\#}\dots\hat{b}_{j'}^{\#}\left(\hat{a}_{S}\right)^{n}\rho\right] = \operatorname{tr}\left[\left(\hat{a}_{S}^{\dagger}\right)^{n}\left(\hat{a}_{S}\right)^{n}\rho\right]\operatorname{tr}\left[\hat{b}_{1}^{\#}\dots\hat{b}_{j'}^{\#}\rho\right]. \tag{B.7}$$

When we then take into account the denominator in equation (B.6), we find

$$\langle \hat{b}_{1}^{\#} \dots \hat{b}_{j'}^{\#} \rangle = \text{tr} \left[\hat{b}_{1}^{\#} \dots \hat{b}_{j'}^{\#} \rho \right],$$
 (B.8)

it automatically follows that $\langle \hat{Y} \rangle = \text{tr}[\hat{Y} \rho]$. The expectation value $\langle \hat{a}_1^\# \dots \hat{a}_j^\# \rangle$ is much more intricate to evaluate since by construction either $\operatorname{tr}[\hat{a}_{k}^{\dagger}\hat{a}_{S}\rho]\neq0$ or $\operatorname{tr}[\hat{a}_{k}\hat{a}_{S}\rho]\neq0$. We then find

$$\operatorname{tr}\left[\left(\hat{a}_{S}^{\dagger}\right)^{n}\hat{a}_{1}^{\#}\dots\hat{a}_{j}^{\#}\left(\hat{a}_{S}\right)^{n}\rho\right] = \sum_{\mathcal{P}}\prod_{\{p_{1},p_{2}\}\in\mathcal{P}}\operatorname{tr}\left[\hat{a}_{p_{1}}^{\#}\hat{a}_{p_{2}}^{\#}\rho\right] = \operatorname{tr}\left[\left(\hat{a}_{S}^{\dagger}\right)^{n}\left(\hat{a}_{S}\right)^{n}\rho\right]\operatorname{tr}\left[\hat{a}_{1}^{\#}\dots\hat{a}_{j}^{\#}\rho\right] + \operatorname{cross terms}.$$
(B.9)

We therefore find that

$$\langle \hat{a}_1^{\#} \dots \hat{a}_j^{\#} \rangle = \operatorname{tr} \left[\hat{a}_1^{\#} \dots \hat{a}_j^{\#} \rho \right] + \mathcal{T}.$$
 (B.10)

The cross terms $\mathcal T$ contain expectation values that combine creation or annihilation operators of the Wick monomial $\hat{a}_1^{\#} \dots \hat{a}_i^{\#}$ with either \hat{a}_S or \hat{a}_S^{\dagger} as obtained from the perfect matching (equation (B.9)). For what follows, it is useful to explicitly identify these cross terms as

$$\mathcal{T} = \langle \hat{a}_1^{\#} \dots \hat{a}_i^{\#} \rangle - \operatorname{tr} \left[\hat{a}_1^{\#} \dots \hat{a}_i^{\#} \rho \right]. \tag{B.11}$$

Finally, we can now consider $\langle \hat{a}_1^{\#} \dots \hat{a}_j^{\#} \hat{b}_1^{\#} \dots \hat{b}_{j'}^{\#} \rangle$ and apply many of the same lines of reasoning. We express

$$\operatorname{tr}\left[\left(\hat{a}_{S}^{\dagger}\right)^{n}\hat{a}_{1}^{\#}\dots\hat{a}_{j}^{\#}\hat{b}_{1}^{\#}\dots\hat{b}_{j'}^{\#}\left(\hat{a}_{S}\right)^{n}\rho\right]=\sum_{\mathcal{P}}\prod_{\{p_{1},p_{2}\}\in\mathcal{P}}\operatorname{tr}\left[\hat{a}_{p_{1}}^{\#}\hat{a}_{p_{2}}^{\#}\rho\right],$$

where $\hat{a}_{p_i}^\#$ can either be a creation/annihilation operator of the type \hat{a} or of the type \hat{b} . A wide variety of terms will appear in the set of perfect matchings (equation (B.12)). Generally speaking, we have the terms related to $\hat{a}_1^\# \dots \hat{a}_j^\#$, those related to photon subtraction, i.e. \hat{a}_S or \hat{a}_S^\dagger , and those related to $\hat{b}_1^\# \dots \hat{b}_j^\#$. The crucial element is that $\mathrm{tr}[[\rho]\hat{b}_k^\dagger\hat{a}_S]=0$ and $\mathrm{tr}[[\rho]\hat{b}_k\hat{a}_S]=0$, which implies that any perfect matching that matches a subtraction operator \hat{a}_S or \hat{a}_S^\dagger with a creation or annihilation operator that originates from $\hat{b}_1^\# \dots \hat{b}_{j'}^\#$ vanishes. In other words, the subtraction operators \hat{a}_S or \hat{a}_S^\dagger can be matched only with creation and annihilation operators that live on $\mathcal{A}_{\mathrm{near}}$. This implies that we can rewrite

$$\frac{\operatorname{tr}\left[\left(\hat{a}_{S}^{\dagger}\right)^{n}\hat{a}_{1}^{\#}\dots\hat{a}_{j}^{\#}\hat{b}_{1}^{\#}\dots\hat{b}_{j'}^{\#}\left(\hat{a}_{S}\right)^{n}\rho\right]}{\operatorname{tr}\left[\left(\hat{a}_{S}^{\dagger}\right)^{n}\left(\hat{a}_{S}\right)^{n}\rho\right]} = \operatorname{tr}\left[\hat{a}_{1}^{\#}\dots\hat{a}_{j}^{\#}\hat{b}_{1}^{\#}\dots\hat{b}_{j'}^{\#}\rho\right] + \frac{\operatorname{tr}\left[\hat{b}_{1}^{\#}\dots\hat{b}_{j'}^{\#}\rho\right]\operatorname{tr}\left[\left(\hat{a}_{S}^{\dagger}\right)^{n}\hat{a}_{1}^{\#}\dots\hat{a}_{j}^{\#}\left(\hat{a}_{S}\right)^{n}\rho\right]}{\operatorname{tr}\left[\left(\hat{a}_{S}^{\dagger}\right)^{n}\left(\hat{a}_{S}\right)^{n}\rho\right]} - \operatorname{tr}\left[\hat{a}_{1}^{\#}\dots\hat{a}_{j}^{\#}\rho\right]\operatorname{tr}\left[\hat{b}_{1}^{\#}\dots\hat{b}_{j'}^{\#}\rho\right] \\
= \operatorname{tr}\left[\hat{a}_{1}^{\#}\dots\hat{a}_{j}^{\#}\hat{b}_{1}^{\#}\dots\hat{b}_{j'}^{\#}\rho\right] + \operatorname{tr}\left[\hat{b}_{1}^{\#}\dots\hat{b}_{j'}^{\#}\rho\right]\langle\hat{a}_{1}^{\#}\dots\hat{a}_{j}^{\#}\rangle \\
- \operatorname{tr}\left[\hat{a}_{1}^{\#}\dots\hat{a}_{j}^{\#}\rho\right]\operatorname{tr}\left[\hat{b}_{1}^{\#}\dots\hat{b}_{j'}^{\#}\rho\right]. \tag{B.13}$$

where the term $\operatorname{tr}[\hat{a}_1^{\#} \dots \hat{a}_j^{\#} \rho] \operatorname{tr}[\hat{b}_1^{\#} \dots \hat{b}_{j'}^{\#} \rho]$ is subtracted to avoid double counting. We can then use the definition of the cross terms (B.11) to write

$$\langle \hat{a}_{1}^{\#} \dots \hat{a}_{i}^{\#} \hat{b}_{1}^{\#} \dots \hat{b}_{i'}^{\#} \rangle = \operatorname{tr}[\hat{a}_{1}^{\#} \dots \hat{a}_{i}^{\#} \hat{b}_{1}^{\#} \dots \hat{b}_{i'}^{\#} \rho] + \mathcal{T} \operatorname{tr}[\hat{b}_{1}^{\#} \dots \hat{b}_{i'}^{\#} \rho]. \tag{B.14}$$

This provides us with the final ingredient we need to complete the proof.

When the results (B.8), (B.10), and (B.14) are combined, we find that all terms proportional to \mathcal{T} drop out. As such, we find indeed that the identity (B.5) holds. Because the identity holds for all possible Wick monomials, it follows that

$$\langle \hat{X}\hat{Y}\rangle - \langle \hat{X}\rangle \langle \hat{Y}\rangle = \text{tr}[\hat{X}\hat{Y}\rho] - \text{tr}[\hat{X}\rho]\text{tr}[\hat{Y}\rho], \tag{B.15}$$

for any par of observables $\hat{X} \in \mathcal{A}_{near}$ and $\hat{Y} \in \mathcal{A}_{far}$.

In full analogy, one can prove a second theorem

Theorem B.2. For any observables $\hat{X}, \hat{Y} \in \mathcal{A}_{far}$, it holds that

$$\langle \hat{X}\hat{Y}\rangle - \langle \hat{X}\rangle \langle \hat{Y}\rangle = \text{tr}[\hat{X}\hat{Y}\rho] - \text{tr}[\hat{X}\rho]\text{tr}[\hat{Y}\rho], \tag{B.16}$$

where $\langle ... \rangle$ denotes the expectation value in the n-photon subtracted state and $tr[...\rho]$ is the expectation value in the initial Gaussian state.

Proof. The proof is fully analogous to theorem B.1. The only modification it that in the present case the cross terms all vanish, such that $\mathcal{T} = 0$.

Appendix C. Moment analysis

To provide a complementary quantitative grasp on the statistics of the degrees and clustering coefficients of the emergent networks of photon-number correlations as defined in equation (4), we analyzed the moments of these distributions. More specifically, we considered the first four non-trivial moments: mean, variance, skew, and kurtosis. For an arbitrary stochastic variable *X*, these quantities are defined as

$$Mean = \mathbb{E}[X], \tag{C.1}$$

$$Variance = \mathbb{E}[(X - \mathbb{E}[X])^2], \tag{C.2}$$

Skewness =
$$\frac{\mathbb{E}[(X - \mathbb{E}[X])^3]}{\mathbb{E}[(X - \mathbb{E}[X])^2]^{3/2}},$$
 (C.3)

$$Kurtosis = \frac{\mathbb{E}[(X - \mathbb{E}[X])^4]}{\mathbb{E}[(X - \mathbb{E}[X])^2]^2},$$
(C.4)

and thus they can be estimated from the data. Furthermore, we used error propagation methods to estimate the standard statistical error on each of these quantities.

ORCID iDs

References

- [1] Islam R, Ma R, Preiss P M, Eric Tai M, Lukin A, Rispoli M and Greiner M 2015 Nature 528 77-83
- [2] Laflorencie N 2016 Quantum entanglement in condensed matter systems Phys. Rep. 646 1-59
- [3] Asavanant W et al 2019 Science 366 373-6
- [4] Larsen M V, Guo X, Breum C R, Neergaard-Nielsen J S and Andersen U L 2019 Science 366 369-72
- [5] Chen M, Menicucci N C and Pfister O 2014 Phys. Rev. Lett. 112 120505
- [6] Ra Y-S, Dufour A, Walschaers M, Jacquard C, Michel T, Fabre C and Treps N 2020 Nat. Phys. 16 144-7
- [7] Biagi N, Costanzo L S, Bellini M and Zavatta A 2020 Phys. Rev. Lett. 124 033604
- [8] Walschaers M, Fabre C, Parigi V and Treps N 2017 Phys. Rev. A 96 053835
- [9] Zhuang Q, Shor P W and Shapiro J H 2018 Phys. Rev. A 97 052317
- [10] Albarelli F, Genoni M G, Paris M G A and Ferraro A 2018 Phys. Rev. A 98 052350
- [11] Takagi R and Zhuang Q 2018 Phys. Rev. A 97 062337
- [12] Cimini V, Barbieri M, Treps N, Walschaers M and Parigi V 2020 Phys. Rev. Lett. 125 160504
- [13] Walschaers M, Parigi V and Treps N 2020 PRX Quantum 1 020305
- [14] Chabaud U, Douce T, Markham D, van Loock P, Kashefi E and Ferrini G 2017 Phys. Rev. A 96 062307
- [15] Hamilton C S, Kruse R, Sansoni L, Barkhofen S, Silberhorn C and Jex I 2017 Phys. Rev. Lett. 119 170501
- [16] Aaronson S and Arkhipov A 2011 The computational complexity of linear optics Proc. 53rd Annual ACM Symp. on Theory of Computing (STOC '11) (New York, USA) (New York, USA Association for Computing Machinery) pp 333–42
- [17] Gagatsos C N and Guha S 2019 Phys. Rev. A 99 053816
- [18] Zhong H-S et al 2020 Science **370** 1460–3
- [19] Zhong H S etal 2021 Phys. Rev. Lett. 127 180502
- [20] Madsen L S et al 2022 Nature **606** 75–81
- [21] Chabaud U and Walschaers M 2023 Phys. Rev. Lett. 130 090602
- [22] Walschaers M, Kuipers J, Urbina J-D, Mayer K, Tichy M C, Richter K and Buchleitner A 2016 New J. Phys. 18 032001
- [23] Giordani T et al 2018 Nat. Photon. 12 173-8
- [24] Phillips D S, Walschaers M, Renema J J, Walmsley I A, Treps N and Sperling J 2019 *Phys. Rev.* A 99 023836
- [25] Cardin Y and Quesada N 2022 Photon-number moments and cumulants of Gaussian states (arXiv:2212.06067)
- [26] Cai Y, Roslund J, Ferrini G, Arzani F, Xu X, Fabre C and Treps N 2017 Nat. Commun. 8 15645
- [27] Nokkala J, Arzani F, Galve F, Zambrini R, Maniscalco S, Piilo J, Treps N and Parigi V 2018 New J. Phys. 20 053024
- [28] Sansavini F and Parigi V 2020 Entropy 22 26
- [29] Arzani F, Ferrini G, Grosshans F and Markham D 2019 Phys. Rev. A 100 022303
- [30] Roslund J, Medeiros de Araújo R, Jiang S, Fabre C and Treps N 2014 Nat. Photon. 8 109
- [31] Yokoyama S, Ukai R, Armstrong S C, Sornphiphatphong C, Kaji T, Suzuki S, Yoshikawa J-I, Yonezawa H, Menicucci N C and Furusawa A 2013 Nat. Photon. 7 982
- [32] Menicucci N C, van Loock P, Gu M, Weedbrook C, Ralph T C and Nielsen M A 2006 Phys. Rev. Lett. 97 110501
- [33] Gu M, Weedbrook C, Menicucci N C, Ralph T C and van Loock P 2009 Phys. Rev. A 79 062318
- [34] Walschaers M, Sarkar S, Parigi V and Treps N 2018 Phys. Rev. Lett. 121 220501
- $[35] \ \ Newman\ M \ E\ J\ 2018\ \textit{Networks}\ 2nd\ edn\ (Oxford: Oxford\ University\ Press)$
- [36] Barabási A L 2016 Networks Science (Cambridge: Cambridge University Press)
- [37] Albert R and Barabási A L 2002 Rev. Mod. Phys. 74 47-97
- [38] Dorogovtsev S N, Goltsev A V and Mendes J F F 2008 Rev. Mod. Phys. 80 1275-335
- [39] Bianconi G 2015 Europhys. Lett. 111 56001
- [40] Halu A, Garnerone S, Vezzani A and Bianconi G 2013 Phys. Rev. E 87 022104
- [41] Jahnke L, Kantelhardt J W, Berkovits R and Havlin S 2008 Phys. Rev. Lett. 101 175702
- [42] Burioni R, Cassi D, Rasetti M, Sodano P and Vezzani A 2001 J. Phys. B: At. Mol. Opt. Phys. 34 4697-710
- [43] Mülken O and Blumen A 2011 Phys. Rep. 502 37-87
- [44] Valdez M A, Jaschke D, Vargas D L and Carr L D 2017 Phys. Rev. Lett. 119 225301
- [45] Nokkala J, Maniscalco S and Piilo J 2018 Sci. Rep. 8 13010
- [46] Biamonte J, Faccin M and De Domenico M 2019 Commun. Phys. 2 53
- [47] Cabot A, Galve F, Eguíluz V M, Klemm K, Maniscalco S and Zambrini R 2018 npj Quantum Inf. 4 57
- [48] Chakraborty S, Novo L, Ambainis A and Omar Y 2016 Phys. Rev. Lett. 116 100501

- [49] Cuquet M and Calsamiglia J 2009 Phys. Rev. Lett. 103 240503
- [50] Faccin M, Migdał P, Johnson T H, Bergholm V and Biamonte J D 2014 Phys. Rev. X 4 041012
- [51] Sundar B, Valdez M A, Carr L D and Hazzard K R A 2018 Phys. Rev. A 97 052320
- [52] Buča B, Tindall J and Jaksch D 2019 Nat. Commun. 10 1730
- [53] Sokolov B, Rossi M A C, García-Pérez G and Maniscalco S 2022 Phil. Trans. R. Soc. A 380 20200421
- [54] Hillberry L E, Jones M T, Vargas D L, Rall P, Halpern N Y, Bao N, Notarnicola S, Montangero S and Carr L D 2021 Quantum Sci. Technol. 6 045017
- [55] Kimble H J 2008 Nature 453 1023-30
- [56] Childs A M 2009 Phys. Rev. Lett. 102 180501
- [57] Mohseni M, Rebentrost P, Lloyd S and Aspuru-Guzik A 2008 J. Chem. Phys. 129 174106
- [58] Plenio M B and Huelga S F 2008 New J. Phys. 10 113019
- [59] Walschaers M, Schlawin F, Wellens T and Buchleitner A 2016 Annu. Rev. Condens. Matter Phys. 7 223-48
- [60] Awschalom D et al 2021 PRX Quantum 2 017002
- [61] Altman E et al 2021 PRX Quantum 2 017003
- [62] Raussendorf R and Briegel H J 2001 Phys. Rev. Lett. 86 5188-91
- [63] Raussendorf R, Browne D E and Briegel H J 2003 Phys. Rev. A 68 022312
- [64] Fabre C and Treps N 2020 Rev. Mod. Phys. 92 035005
- [65] Verbeure A F 2011 Bose Systems (London: Springer) pp 7–26
- [66] Menicucci N C, Flammia S T and van Loock P 2011 Phys. Rev. A 83 042335
- [67] Briegel H J and Raussendorf R 2001 Phys. Rev. Lett. 86 910-3
- [68] Van den Nest M, Miyake A, Dür W and Briegel H J 2006 Phys. Rev. Lett. 97 150504
- [69] Walschaers M, Fabre C, Parigi V and Treps N 2017 Phys. Rev. Lett. 119 183601
- [70] Walschaers M and Treps N 2020 Phys. Rev. Lett. 124 150501
- [71] Ra Y S, Jacquard C, Dufour A, Fabre C and Treps N 2017 Phys. Rev. X 7 031012
- [72] Wenger J, Tualle-Brouri R and Grangier P 2004 Phys. Rev. Lett. 92 153601
- [73] Parigi V, Zavatta A, Kim M and Bellini M 2007 Science 317 1890-3
- [74] Zavatta A, Viciani S and Bellini M 2004 Science 306 660-2
- [75] Lvovsky A I, Grangier P, Ourjoumtsev A, Parigi V, Sasaki M and Tualle-Brouri R Production and applications of non-Gaussian quantum states of light (arXiv:2006.16985)
- [76] Arzani F, Treps N and Ferrini G 2017 Phys. Rev. A 95 052352
- [77] Yukawa M, Miyata K, Yonezawa H, Marek P, Filip R and Furusawa A 2013 Phys. Rev. A 88 053816
- [78] Navarrete-Benlloch C, García-Patrón R, Shapiro J H and Cerf N J 2012 Phys. Rev. A 86 012328
- [79] Deshpande A et al 2022 Sci. Adv. 8 eabi7894
- [80] Walschaers M 2021 Code: Cv quantum complex networks (version 2) (available at: https://archive.softwareheritage.org/browse/origin/directory/?origin_url=https://github.com/mwalschaers/ComplexNetworks)